NAA-SR-6118
COPY

HALLAM EXPONENTIAL EXPERIMENTS USING U-Mo FUEL

AEC Research and Development Report

ATOMICS INTERNATIONAL
A DIVISION OF NORTH AMERICAN AVIATION, INC.

DISCLAIMER

LEGAL NOTICE

Price $1.25
Available from the Office of Technical Services
Department of Commerce
Washington 25, D. C.

NAA-SR-6118
REACTOR TECHNOLOGY
52 PAGES

HALLAM EXPONENTIAL EXPERIMENTS USING U-Mo FUEL

By
C. R. HILLIG

ATOMICS INTERNATIONAL
A DIVISION OF NORTH AMERICAN AVIATION, INC.
P.O. BOX 309 CANOGA PARK, CALIFORNIA

CONTRACT: AT(11-1)-GEN-8
ISSUED:
SEP 15 1961

DISTRIBUTION

This report has been distributed according to the category "Reactor Technology" as given in "Standard Distribution Lists for Unclassified Scientific and Technical Reports" TID-4500 (16th Ed.), December 15, 1960. A total of 650 copies was printed.

ACKNOWLEDGMENT

The author is grateful to G. L. Blackshaw and D. J. Miller for their assistance in securing the foil activation data and for operation of the AE-6 reactor, to Mrs. C. S. Johnston for so ably handling the counting room operations, and to R. K. Paschall for assistance in data analysis. The author wishes to thank Dr. C. H. Skeen for his contributions to the capture and fission ratio measurements, and most of all wishes to thank Dr. W. W. Brown for his assistance in planning the experiments.

CONTENTS

TABLES

TABLES

FIGURES

FIGURES

ABSTRACT

The results of exponential experiments with graphite-moderated lattices containing multirod fuel clusters are presented. Three lattices of different spacings where the fuel clusters form regular hexagons, and one square lattice were studied. Fuel clusters were of a uranium molybdenum alloy. Some measurements were also made using a single uranium carbide fuel cluster and a uranium molybdenum fuel element of lower U^{235} enrichment. The results are presented for measurements of thermal neutron diffusion length (L) of the moderator in each assembly, material buckling (B^2) for the various lattices, detailed neutron flux distributions, thermal utilization, (f) and the ratios involved in resonance escape probability (r_p) and fast effect (r_ϵ). The results are presented in detail in this report so they can be used as a comparison for theoretical calculations and therefore aid in improving calculational models.

I. INTRODUCTION

For the first fuel loading of the sodium-cooled, graphite-moderated reactor in the Hallam Nuclear Power Facility (HNPF),[1] a U-Mo alloy is to be used. Because the reactor core design differs substantially from other sodium graphite reactors for which experimental details are available, exponential experiments were performed to provide some firm data on which to base calculations for the reactor core. The design of the reactor includes multi-rod fuel clusters loaded at the vertices of regular hexagons (hexagonal lattice). The distance across the flats of the hexagons formed by the fuel clusters is 16 in. The U-Mo alloy fuel is contained in stainless steel tubes, and the clusters of fuel rods are inserted into Zircaloy process tubes. The moderator cell is a graphite log, hexagonal in cross section with scalloped corners, contained in type 304 stainless steel cladding. The coolant, sodium, flows through the fuel clusters and between the graphite moderator logs.

Because of the difficulty in making calculations for this type geometry and other uncertainties such as the value of the resonance integral of molybdenum, the reactor core was mocked-up as closely as practical in an exponential lattice and the lattice parameters were measured. Measurements were also made in assemblies where the lattice spacing was different from that of the HNPF reactor. This included measurements in three hexagonal lattices and one square lattice. The purpose was to supply experimental results for several fuel to moderator ratios as a check for theoretical calculations and to compare the square array of fuel clusters to the hexagonal array. Some measurements were also made in a single U-Mo fuel cluster of lower U^{235} enrichment and a single 12-rod UC fuel element. The measurements using the UC fuel element were made to support studies being carried out to determine the requirements for a second core loading using UC fuel.

The experimental measurements consisted of determining the neutron flux distributions for each assembly, with and without fuel, in both horizontal directions and along the vertical axis. From the analysis of these results the material buckling (B^2) for each lattice loaded with U-Mo alloy fuel was obtained and the thermal neutron diffusion length (L) of the moderator for each solid graphite stack was determined. Detailed measurements were made of the neutron flux distributions within a lattice cell, and the average flux in each material of the

cell was calculated. These detailed intracell measurements were made in each hexagonal lattice using the U-Mo alloy fuel and in one lattice using the single element of lower U^{235} enriched U-Mo fuel and the UC fuel. From these, values of thermal utilization (f) were obtained. Also measurements were made in the hexagonal lattices to determine the ratios of resonance to thermal capture probabilities (r_p) in U^{238}, and the U^{238} fissions to the U^{235} fissions (r_ϵ) for the HNPF type U-Mo fuel clusters and UC fuel cluster. These results are herewith presented, together with graphs of typical neutron flux distributions.

These results have been used as a basis for checking calculational models used to determine the enrichment to be used for the HNPF reactor. The detailed intracell neutron flux distributions have been used to aid in solving some of the heat transfer problems.

II. PHYSICAL DESCRIPTION OF THE EXPONENTIAL ASSEMBLIES

A sketch of the AE-6 Reactor with an exponential assembly on the reactor thermal column is shown in Figure 1. The AE-6 water boiler reactor and the

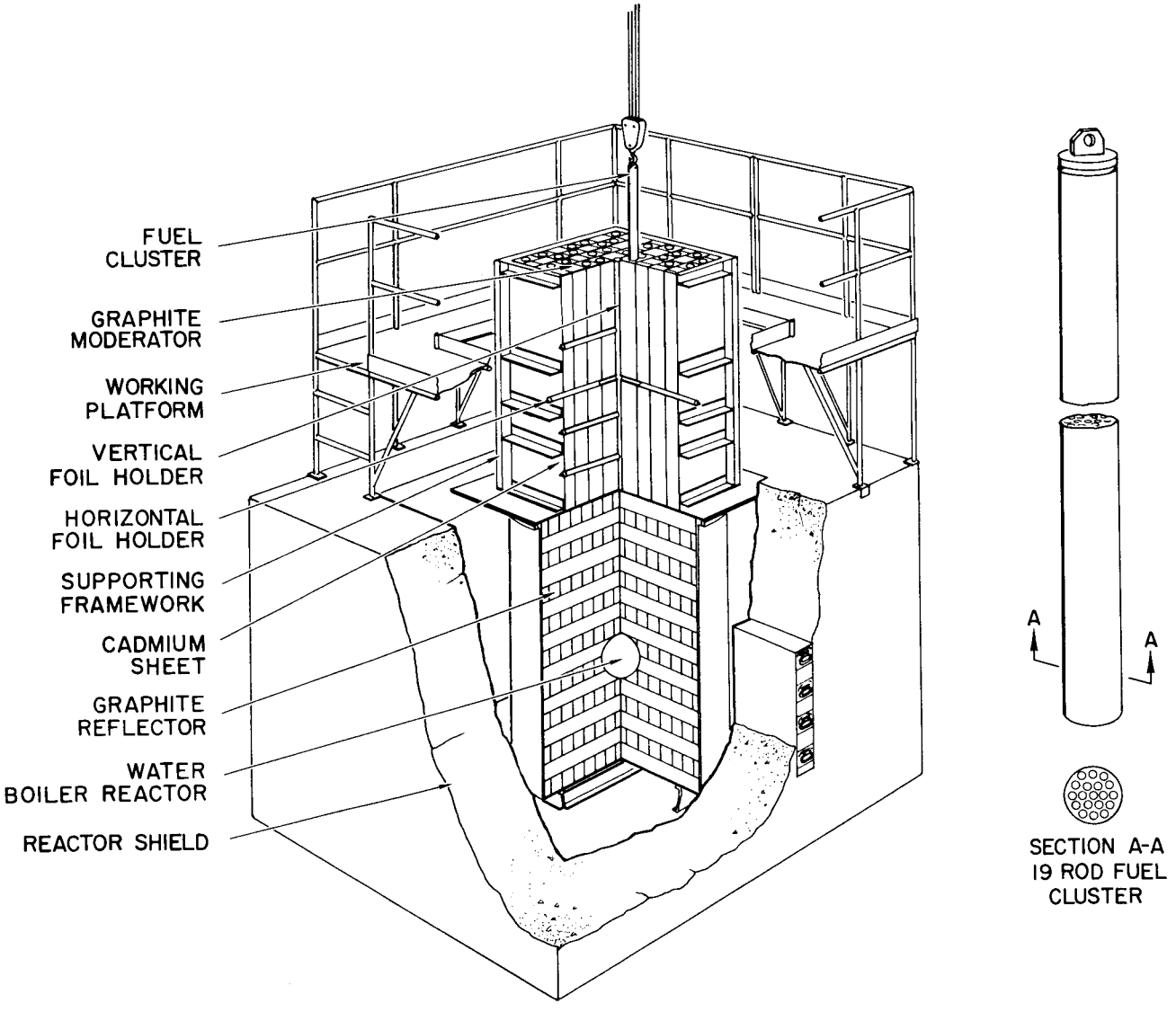

Figure 1. Cutaway View of Exponential Assembly and Water Boiler Reactor

vertical thermal column[2] supply the thermal neutrons to the exponential assembly. The thermal column is 5 ft in diameter. The thermal neutron flux at the top of the thermal column is approximately 5 by 10^5 n/cm^2-sec-w giving a maximum neutron flux of about 10^9 n/cm^2-sec for the maximum operating power of the reactor. As can be seen from the sketch, the assemblies are contained by a cadmium sheet. This cadmium sheet serves as definite boundaries on the four

sides for thermal neutrons. Graphite blocks and fuel clusters can be loaded into or removed from the assembly by use of the overhead crane.

The graphite moderator blocks in the assembly were 69 in. high. The graphite was machined to provide channels for the fuel clusters, these holes being 4.75 in. in diameter. The graphite dimensions were designed to allow stacking a basic assembly where fuel channels are at the vertices of regular hexagons, the distance across the flats of the hexagons being 13 in. By adding spacer blocks the basic assembly could be expanded to allow for fuel channels to be at the vertices of hexagons either 16 in. or 19 in. across the flats. The 16-in. spacing is the same as that proposed for the Hallam reactor. Figure 2 shows the top view of the assembly having the spacing the same as that of the Hallam reactor. Provisions were made to construct one other type lattice. By using the basic blocks of the 13-in., hexagonal-type assembly with special spacers, an array of square lattice cells could be obtained where the cells were 9.5 in. on a side. A top view of this assembly is shown in Figure 3. Table 1 lists the

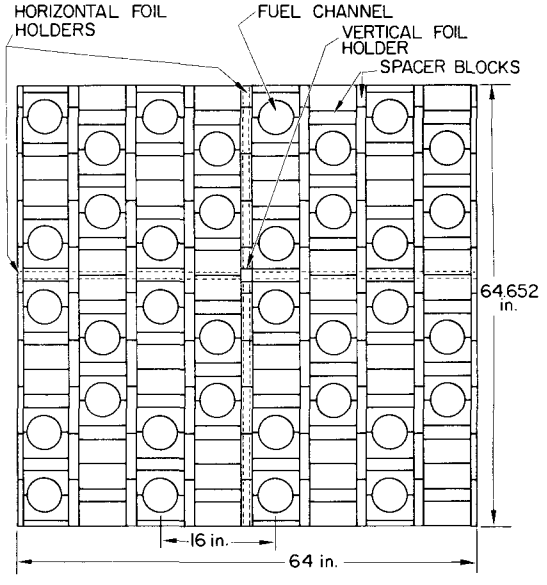

Figure 2. Sixteen-Inch Hexagonal-Type Assembly

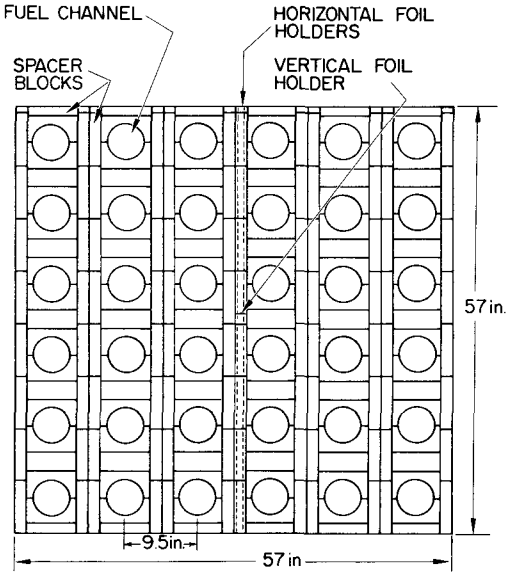

Figure 3. Nine-and-One-Half-Inch Square-Type Assembly

dimensions of each assembly and the number of fuel channels available for each assembly. For brevity, the different assemblies are to be referred to as the 9-1/2-in. square, 13-in., 16-in, and 19-in. assemblies or lattices throughout the remainder of this report. Graphite filler plugs, 69 in. long by 4.742-in. diameter, were provided to fill the empty fuel channels. With these filler plugs in place, a solid graphite stack was obtainable for each assembly.

TABLE I

ASSEMBLY DIMENSIONS AND NUMBER OF FUEL CHANNELS

Assembly	X, Width (in.)	Y, Width (in.)	Z, Height (in.)	Number of Fuel Channels
13 in. hexagonal	52.000	52.528	69	36
16 in. hexagonal	64.000	64.652	69	36
19 in. hexagonal	66.500	65.808	69	28
9-1/2 in. square	57.000	57.000	69	36

In the actual Hallam reactor core[1] the fuel slugs are to be contained in stainless steel tubes, and sodium coolant will flow through the fuel clusters. Also zirconium and stainless steel are to be used for process tubes and moderator cladding. Because it was not practical to mockup the structural materials for the exponential experiments, they were omitted except for one measurement. This measurement will be discussed in Section VII.

The sodium around the fuel elements was mocked-up using aluminum because the two materials have similar properties for thermal neutrons, the aluminum is easily obtained, has no long-lived radioactive products, is easily machined, and provides an adequate mockup for the sodium used in the actual reactor. The macroscopic absorption and scattering cross sections of the aluminum used are 0.0146 cm^{-1} and 0.0834 cm^{-1} respectively, compared to values for sodium of 0.013 cm^{-1} and 0.089 cm^{-1}. Figure 4 shows a picture of the fuel holder. The fuel holders consist of 1100F aluminum cylinders, 4-3/4 in. in diameter by 66 in. long with 19 holes drilled parallel to the axis of the cylinders. They have 1/2-in. base plates and 1/2-in. caps with lifting lugs, both made of aluminum.

Four different fuel clusters were studied. The majority of the measurements were performed using a fuel cluster with the design proposed for the Hallam reactor. That is a 19-rod, 3-1/2 w/o enriched U - 10 w/o Mo cluster. Figure 5 shows this fuel cluster. The 3-1/2 w/o enriched U - 10 Mo as-cast slugs were made in 12-in. lengths and 6-in. lengths. The slugs were cast to a 0.590 ± 0.005 in. diameter specification. The average diameter of the slugs was checked as 0.592-in. The fuel slugs were loaded into the holes of the aluminum holders to give a fuel height of 66 ± 1/4 in. and a fuel area of about 5.2 $in.^2$. The average composition of the slugs is 10.15 w/o Mo and 89.85 w/o U with an enrichment of 3.448 w/o U^{235}. A detailed description of the fuel slugs can be obtained from Reference 3.

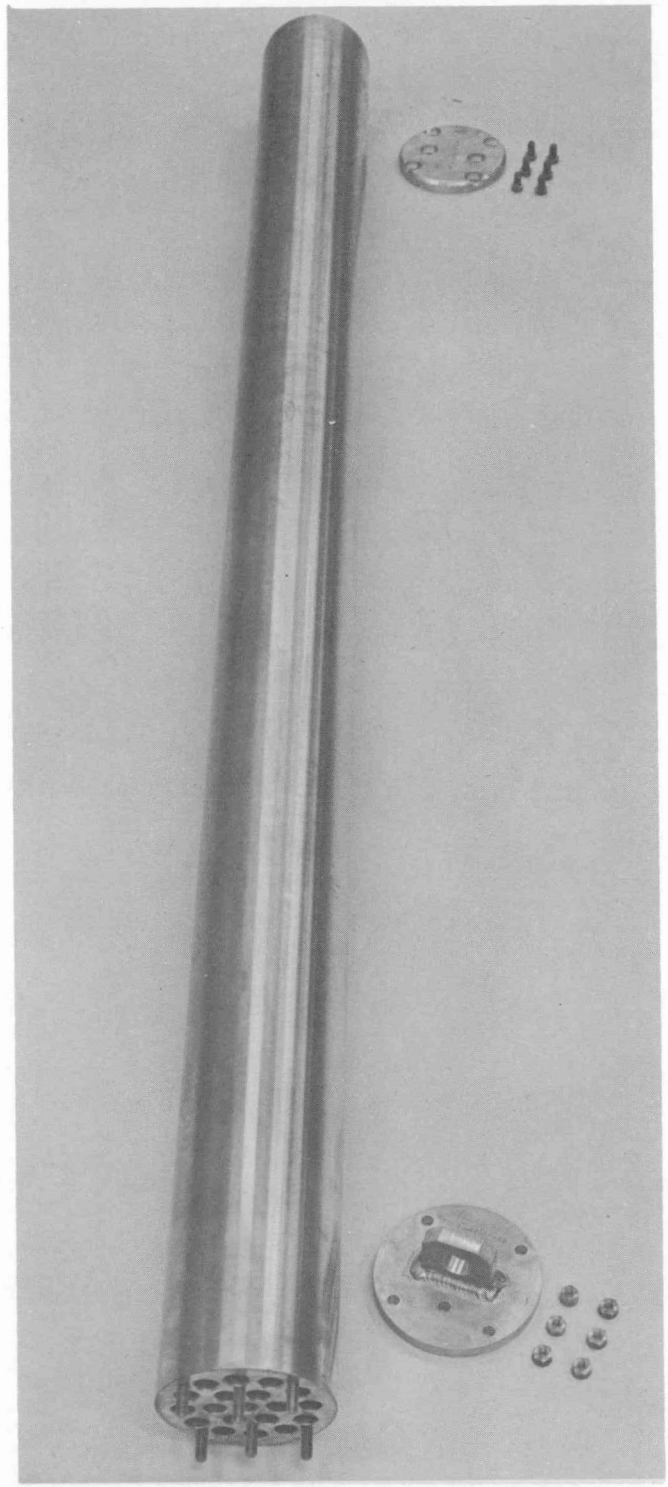

Figure 4. Aluminum Fuel Holder

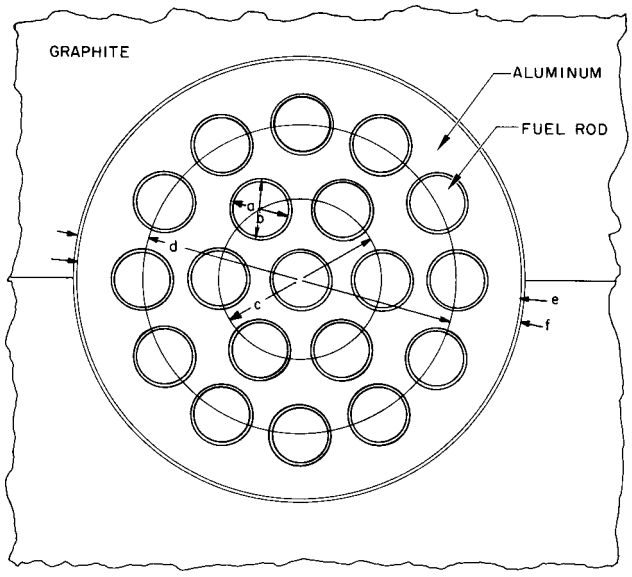

Figure 5. Cross Sectional View of Fuel Cluster With Dimensions

Fuel Composition	86.75	w/o U^{238}	a. fuel rod, 0.592-in. diameter
	3.10	w/o U^{235}	b. aluminum hole, 0.606-in. diameter
	10.15	w/o Mo	c. inner ring location, 1.654-in. diameter
Fuel Density	17.12	gm/cm^3	d. outer ring location, 3.320-in. diameter
Aluminum Density	2.67	gm/cm^3	e. aluminum cluster, 4.742-in. diameter
Graphite Density	1.685	gm/cm^3	f. graphite moderator fuel channel hole, 4.755-in. diameter

Other fuel clusters studied were a 19-rod, 2.778 w/o enriched U - 10 w/o Mo with the same dimensions as the one described above, an 18-rod, 3-1/2 w/o enriched U - 10 w/o Mo identical to the 19-rod fuel cluster except the central fuel rod is removed, leaving a void and a 12-rod, 3-1/2 w/o enriched UC fuel element. The UC fuel element was made of slugs cast to 0.798-in. diameter loaded into the aluminum holders to give a fuel height of 66-in. and a fuel area of about 6 $in.^2$. The composition of the fuel is 4.95 w/o C and 95.05 w/o U with an enrichment of 3.448 w/o U^{235}. Figure 6 shows the UC fuel cluster.

Pertinent details defining the properties of these fuel clusters and the moderator for each assembly are given in Table II, and in Figures 5 and 6.

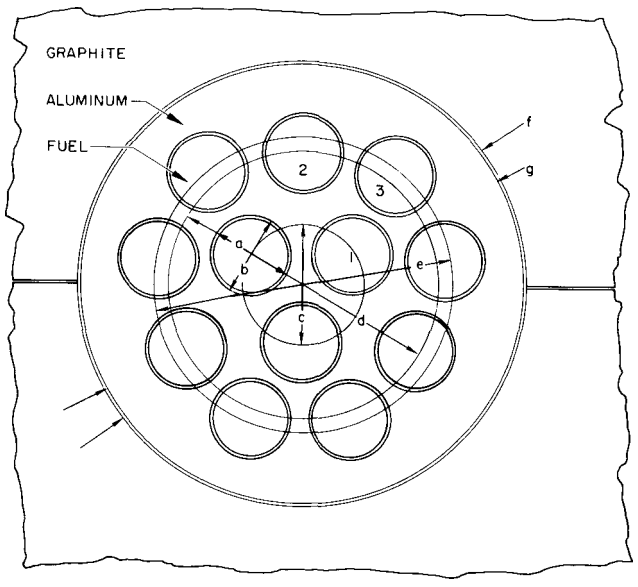

Figure 6. Cross Sectional View of Fuel Cluster With Dimensions

Fuel Composition	91.77	w/o U^{238}
	3.28	w/o U^{235}
	4.95	w/o C
Fuel Density	13.3	gm/cm^3
Aluminum Density	2.67	gm/cm^3
Graphite Density	1.685	gm/cm^3

a. fuel rod, 0.798-in. diameter
b. aluminum hole, 0.807-in. diameter
c. inner ring location, 1.230-in. diameter.
d. second ring location, 2.830-in.diameter
e. outer ring location, 3.090-in. diameter
f. graphite moderator fuel channel, 4.755-in. diameter
g. aluminum cluster, 4.742-in. diameter

TABLE II

MATERIAL DENSITIES AND MICROSCOPIC CROSS SECTIONS FOR EXPONENTIAL LATTICES

Lattice Spacing	Graphite Densities	Graphite Cross Section	Aluminum Densities	Aluminum Cross Section
(in.)	(gm/cm^3)	(mb)	(gm/cm^3)	(mb)
13 hexagonal	1.685 ± 0.005	6.8 ± 0.4	2.67	278
9.5 square	1.684 ± 0.004	7.9 ± 0.4	2.67	278
16 hexagonal	1.679 ± 0.004	8.6 ± 0.5	2.67	278
19 hexagonal	1.694 ± 0.004	8.6 ± 0.5	2.67	278

III. MEASURING TECHNIQUES

A. THERMAL NEUTRON FLUX MEASUREMENTS

The thermal neutron flux distributions used to determine diffusion length, material buckling, and thermal utilization in the graphite assemblies and the fueled lattices were determined by activating small detector foils. The foils were made into two sets. One type was 1 cm^2 by 0.005 in. thick, and the other type was 1 cm by 2 mm by 0.005 in. thick. Their composition is 15% by weight dysprosium oxide dispersed in aluminum. Foils of a given type were calibrated and intercalibrated by exposing them on a rotating disc to neutrons from the AE-6 reactor and then measuring their beta activities. The reproducibility of the calibration of a foil was found to be within 0.15%. The 1-cm^2 foils were exposed in the graphite assemblies in the vertical and horizontal directions in which these foils were covered with either aluminum or cadmium boxes. This was done to obtain relative total (aluminum covered) and relative epithermal (cadmium covered) neutron fluxes. The small 2-mm by 1-cm foils were exposed in the graphite, aluminum, and fuel in the unit cells to obtain intracell relative thermal and relative epithermal neutron fluxes. A more detailed description of the positioning of these foils will be discussed in the following sections.

After exposing the detector foils in the various assemblies, their relative activities were determined by means of gross beta counting with scintillation counters. These counters consist of photomultiplier tubes with 2-mm-thick anthracene crystals and the other necessary instrumentation. Three counting channels were in operation where 0.1% counting statistics were obtainable.

B. MEASUREMENTS RELATING TO RESONANCE ESCAPE AND FAST EFFECT

Measurements of r_p, the ratio of the resonance capture probability to the thermal capture probability in U^{238} and r_ϵ, the ratio of the U^{238} fission probability to the U^{235} fission probability were made in the hexagonal lattices using the 19-rod U - 10 Mo fuel cluster and the 12-rod UC fuel cluster. These measurements consisted of exposing uranium detector foils (depleted, natural and U^{235}-Al alloy foils) and counting their induced relative activities. Some details of these measurements will be covered in the following two paragraphs.

The counting technique employed for the depleted and the natural uranium detector foils involved differential counting at the 103-kev region and integral

counting above 500 kev for the three type foils. The counting equipment used for these experiments consisted of scintillation counters with 2-1/2-in. diameter by 2-mm Na I crystals. The thin crystals were chosen to reduce the background from high energy gamma rays (because of their low attenuation in these crystals) arising from the fission products when counting the 103-kev x-rays. Because foils of about 0.6 and 0.8 in. diameter were used for this experiment, and it was desired to count their activities without cutting the foils into small pieces, the larger foils were cut into quarters. Thus, counters were set up having constant counting efficiency as a function of radial position for a radius of at least 0.3 in. In order to achieve this constant efficiency, a light pipe arrangement was used.

Counting was done at both 103 kev with a window of several volts to measure the Pu^{239} internal conversion x-ray activities and above 500 kev to determine the fission product activities for this correction. The counting efficiency for the higher energy is poor with this thin crystal system but enough counts were obtainable to have good counting statistics.

C. SOME REMARKS REGARDING THE INTRACELL MEASUREMENTS

Intracell measurements were made in the three hexagonal lattices in a centrally located 19-rod fuel element, the 18-rod fuel element and the UC element. For the purpose of doing intracell measurements, the 13-in. and 16-in. lattices, see Figure 2, were reduced to 31 fuel elements by removing one row of elements and graphite. By doing this the fuel element to be studied could be placed in the geometric center of the lattice. For the 19-in. lattice the geometric center of the lattice was the center of the hexagon formed by the fuel elements. By having the fuel element, in which measurements were to be made, near or at the center, the buckling correction is a minimum and errors introduced by this correction are therefore minimized. The observed data, from measurements, were divided by a factor $\cos\mu_x x \cos\mu_y y$, where x and y are the horizontal coordinates of the data point with reference to the lattice axis, and where μ^2 is the horizontal lattice buckling. This buckling correction transforms the observed data to that which would exist in a fuel element situated in a lattice of infinite extent. All foil activation data included in this report have been corrected in this way.

IV. PROPERTIES OF THE MODERATOR

The graphite used in the Hallam exponential experiments was a mold-grade graphite; the same grade as proposed for the actual reactor. Because the thermal neutron diffusion length (L) is highly dependent on the purity of the graphite, a measurement of this parameter was made for each assembly constructed. For each assembly, the empty fuel channels were filled with the graphite plugs to obtain a solid graphite stack. The horizontal and vertical neutron distributions were then measured by foil activation techniques to obtain the relative total neutron flux and the relative epithermal neutron flux. The difference between these two was taken to find the thermal neutron flux distributions. It was found that the epithermal contribution, after correction of the cadmium covered activities for attenuation of the epithermal neutrons by the cadmium, was less than 0.1% of the total neutron flux, so the measurements of the total neutron flux distributions were used for a very good approximation of the relative values of the thermal neutron flux distributions. These distributions are given by $\sinh \nu(z - h)$ for the vertical direction where z is the height above the bottom of the stack of height h, and $\cos\mu_x(x - w_x) \cos\mu_y(y - w_y)$ for the horizontal direction where x and y are horizontal rectangular coordinates measured from the vertical axis of the stack. The μ's define the effective lateral dimensions of each assembly from which the extrapolated widths are given by π/μ.

ν is a measure of the attenuation of the thermal neutron distribution in the vertical direction. The vertical distribution was measured near the center of each stack. The horizontal distributions were measured at four levels in the x direction, 12, 21, 30, and 45 in. from the bottom of the stack; and at one level in the y direction, 30 in. from the bottom of the stack. There was one exception to this. In the 9.5-in. square assembly provisions were not made to measure the horizontal distribution in the y direction. This was omitted in this case because the assembly was square and the value obtained for the x direction could be used for the y direction.

For each measurement of the thermal neutron diffusion length, the square or rectangular assembly that was placed on the cylindrical thermal column caused a geometric mismatch between the assembly base and the thermal column top. Due to this mismatch, the presence of a third harmonic contribution to the horizontal distribution was detected. The third harmonic decreases[4] with height more

rapidly than does the fundamental term. For this reason, the horizontal distributions were measured at several levels to allow for a correction to the vertical data, by actually determining the attenuation of the third harmonic. This was done in the following manner. The horizontal cosine distributions were measured at the four levels 12, 21, 30, and 45 in. from the bottom of the assembly. The four sets of data were normalized at a distance X, one-third out from the center of the stack to the extrapolated edge where the third harmonic has a zero contribution. At the 45-in. level, which is approximately three diffusion lengths from the geometric mismatch, the amplitude of the third harmonic was assumed to be negligible. So by subtracting the data points at the 45-in. level from the data points at the other levels, the difference represents the third harmonic contribution at each level. The results of this analysis are displayed in Figure 7. The amplitude of the third harmonic at the 12-in. level was found to be about 6% of the amplitude of the fundamental for the case of the greatest mismatch. To apply a systematic correction to the data, the procedure outlined in Reference 4 was used to determine the ratio of the amplitude of the third harmonic to the amplitude of the fundamental, as a function of z (height) using the experimentally determined ratio ϕ_{13}/ϕ_{11} at the 12-in. level as a base.

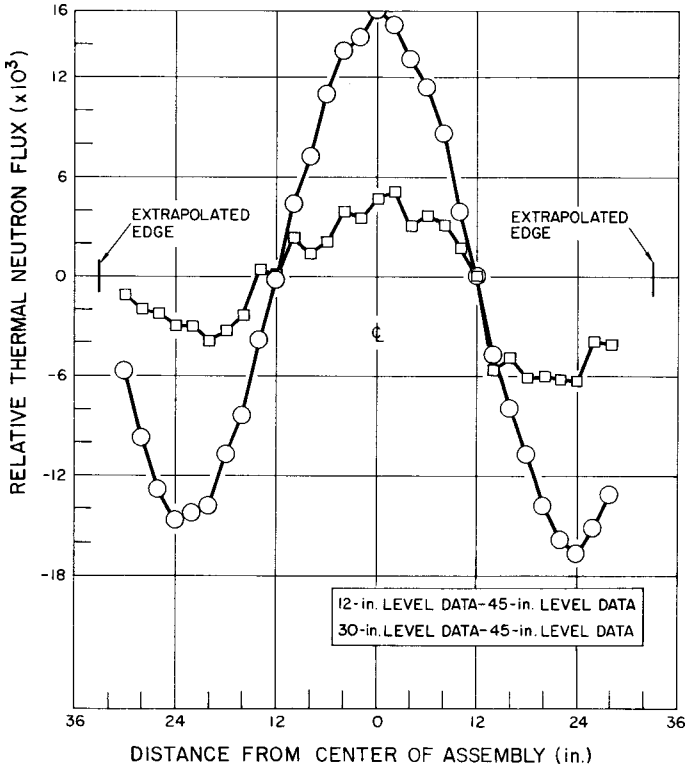

Figure 7. Third Harmonic at Different Levels in Typical Assembly (Amplitude of fundamental equals ~275 x 10^3.)

After making the third harmonic corrections to the data, the data points for each distribution were analyzed using a least squares fit to the sinh function for the vertical thermal neutron distrubtion and a least squares fit to the cosine functions for the horizontal thermal neutron distributions. From these, values of ν, μ_x, and μ_y were determined for each graphite stack. Values of μ_x for the different levels were usually consistent within several tenths of a percent as were values of ν for repeat measurements.

From the values of ν, μ_x, and μ_y for each assembly the thermal diffusion lengths are given by the relation $L^{-2} = \nu^2 - \mu_x^2 - \mu_y^2$. The average density for a graphite stack was obtained by summing the weights of parts and dividing by the graphite assembly volume. Using the determined diffusion length and density, and the microscopic scattering cross section (Σ_s) of 4.8 ± 0.2 mb, a microscopic absorption cross section was calculated for each graphite stack using

$$\Sigma_a = \frac{1}{L^2 3 \Sigma_{tr}} \quad ,$$

where

$$\Sigma_{tr} = \Sigma_s(1 - \mu_o) + \Sigma_a \quad ;$$

here, $\overline{\mu}_o$ is the average cosine of the scattering angle in the lab system, and is given by $\overline{\mu}_o = 2/3$ A. The value of $\overline{\mu}_o$ used for graphite is 0.0555.

From the Σ_a's the microscopic absorption cross sections (σ_a's) were determined for the mold-grade Hallam exponential graphite. The average value of L is 38.2 ± 0.2 cm. The average density for the graphite stack is 1.685 ± 0.004 gm/cm^3. From these two averages, the average σ_a (2200 m/sec) is 8.0 ± 0.4 mb. Table III lists the properties of the graphite in each assembly. If the values of σ_a are compared to the assemblies, it can be seen that as the assemblies are expanded, the σ_a's increase. This would indicate that the spacer blocks might be of poorer grade graphite than the basic blocks.

TABLE III

THERMAL NEUTRON DIFFUSION LENGTH AND OTHER PROPERTIES FOR EACH GRAPHITE ASSEMBLY

Assembly and Number of Fuel Channels	μ_x	μ_y	ν	Diffusion Length, L	Density, ρ	Absorption Cross Section, σ_a, 2200 m/sec
	(m^{-1})	(m^{-1})	(m^{-1})	(cm)	(gm/cm^3)	(mb)
13 in. hexagonal (36)	2.297 ± 0.002	2.313 ± 0.005	4.064 ± 0.008	41.2 ± 0.2	1.685 ± 0.005	6.8 ± 0.4
9.5 in. square (36)	2.126 ± 0.003		3.983 ± 0.014	38.2 ± 0.2	1.684 ± 0.004	7.9 ± 0.4
16 in. hexagonal (36)	1.870 ± 0.002	1.882 ± 0.004	3.790 ± 0.004	36.9 ± 0.1	1.679 ± 0.004	8.6 ± 0.5
16 in. hexagonal (31)	1.875 ± 0.002	2.144 ± 0.004	3.871 ± 0.011	38.2 ± 0.2	1.679 ± 0.004	8.0 ± 0.4
19 in. hexagonal (28)	1.840 ± 0.002	1.820 ± 0.003	3.769 ± 0.004	36.5 ± 0.1	1.694 ± 0.004	8.6 ± 0.5

V. MATERIAL BUCKLING

Measurements similar to those performed in the solid graphite stacks were made in the fueled lattices to determine their material bucklings. The graphite filler plugs were removed from the fuel channels and the fuel elements were loaded into the lattices. The horizontal and vertical components μ_x, μ_y and ν, analogous to those described in the measurements of L, are required for the material buckling, B^2, given by the equation $B^2 = \mu_x^2 + \mu_y^2 - \nu^2$. For all lattices, the horizontal components were taken from the determination of μ_x and μ_y in the diffusion length measurements. It is known that the extrapolated widths are different for a pure moderator assembly as compared to a loaded lattice; but, because the lattices studied here did not have enough repeating cells to allow for a measurement of μ_x and μ_y, values of these parameters obtained from the pure moderator were used in the B^2 determination. If the values of μ_x and μ_y are not greatly in error, the error introduced to the values of B^2 should be small. In order to make an estimate of this error the horizontal traverse in the 9-1/2-in. square lattice was determined where there are six repeating cells across a width. The results of this will be discussed later. The vertical distribution measurement was made over a region of the lattice where the cadmium ratio is constant. To determine this region, for each lattice, indium detector foils were used, both bare and cadmium covered. The cadmium ratio is lower for indium than dysprosium because of the high indium resonance absorption, therefore indium is more desirable for this purpose. Having determined this region, the measurement of the vertical attenuation was performed as described for the determination of L. For the measurement with the fuel present, the epithermal contribution, after correction for the attenuation of the epithermal neutrons by the cadmium, using dysprosium foils, was about 2 or 3% of the total; so for these measurements the epithermal contributions were subtracted from the relative total neutron flux distributions to obtain the relative thermal neutron flux distributions. The values obtained for B^2 for the various lattices are shown graphically in Figure 8 and are listed with the ν values in Table IV. The results will be discussed in the following paragraphs.

The values of B^2 with 19-rod, 3-1/2 w/o U - 10 Mo fuel elements, as can be seen, increased as the moderator-to-fuel ratio increased with a possible maximum value of B^2 between the 16-in. and the 19-in. lattices. The 16-in. lattice is

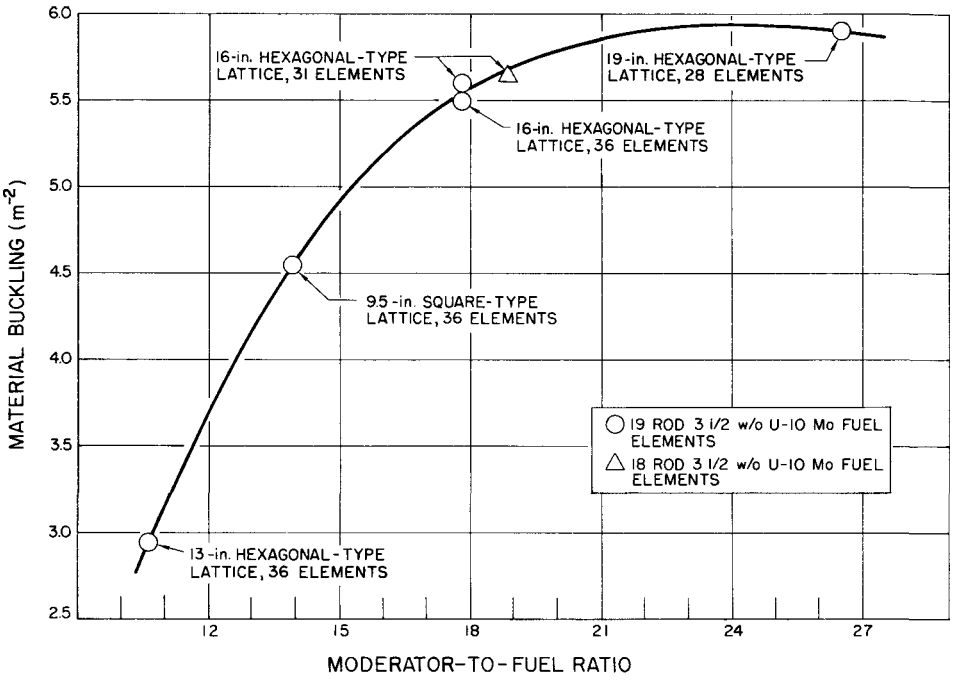

Figure 8. Lattice Bucklings Measured in HNPF Exponential Experiments

TABLE IV

B^2 AND ν IN LATTICES STUDIED CONTAINING 3-1/2 w/o U^{235}, U - 10 Mo FUEL

Lattice	Number of Fuel Rods	ν (m^{-1})	B^2 (m^{-2})
13-in. hexagonal	19	2.772 ± 0.005	2.94 ± 0.04
9.5-in. square	19	2.120 ± 0.006	4.54 ± 0.07
16-in. hexagonal with 36 elements	19	1.241 ± 0.002	5.50 ± 0.07
16-in. hexagonal with 31 elements	19	1.587 ± 0.004	5.60 ± 0.08
16-in. hexagonal	18	1.575 ± 0.003	5.64 ± 0.07
19-in. hexagonal	19	0.889 ± 0.001	5.91 ± 0.09

slightly under-moderated. Two measurements in the 16-in. lattice were made where the only change was the overall size of the lattice. The lattice was reduced from 36 elements to 31 elements to position a fuel channel in the geometric center of the assembly in order to do intracell measurements. This opportunity was taken to check the reproducibility of B^2 for a given lattice spacing in assemblies of different dimensions. The difference observed is small and might be partly due to the difference in moderator properties.

In the 16-in. assembly, with 31-fuel channels, measurements of material buckling were made for both 19-rod and 18-rod fuel elements. These fuel elements were described earlier in the report. After having determined the relative average thermal neutron flux, to be discussed in the next section, for each of the 19 rods of the fuel element, it was suggested that the central rod be omitted and these measurements be repeated. This showed that by leaving a void in the central position of the fuel element the power loss of the 18-rod elements compared to the 19-rod elements was small. It was then desirable to compare bucklings using the different fuel elements. As can be seen from the results, B^2 (19-rod) = 5.60 ± 0.08 m^{-2} and B^2 (18-rod) = 5.64 ± 0.07 m^{-2}, there is no significant difference.

The 9.5-in. square lattice was compared to the hexagonal-type lattices. A square lattice was chosen where its moderator to fuel ratio would fall within the range of the moderator-to-fuel ratios of the hexagonal lattices studied. The material buckling values were compared to determine whether or not the method of grouping the fuel elements, for a given moderator-to-fuel ratio, had a measurable effect on this parameter. It is concluded, the value of the material buckling is not very sensitive to the method of grouping the fuel elements but rather depends only on the fuel-to-moderator ratio for a lattice of uniformly spaced elements.

For the 9.5-in. square lattice, horizontal neutron flux distribution measurements were made to try to determine the μ_x value, which leads to the extrapolated width. This lattice was chosen because it has six repeating cells across a width as can be seen in Figure 3. The method of analysis outlined in the section describing diffusion length measurements was used where points were 9.5 in. apart to be fit to a cosine distribution. The 9.5-in. interval was chosen to fit the flux depressions due to the fuel elements which are 9.5 in. apart. This was done for 10 sets of points, the sets being taken at 1-in. intervals. The average value of these cosine fits was μ_x = 2.097 m^{-2}. The range was from 2.039 to 2.145 m^{-2}. The value used for the buckling determination was the μ_x = 2.126 m^{-2} obtained from the solid graphite stack. This falls within the range of those measured where the fuel was present. It would have been desirable to check this work where more than 6 repeating cells are available, to improve the accuracy of the measurement. It is concluded that the μ_x measured in the pure moderator is accurate within 1% as a value of μ_x for the loaded lattice.

Measurements were made to determine the vertical attenuation, ν, in the 16-in. lattice with six of the fuel elements removed, leaving the fuel element channels void. The purpose of this was to supply some information about the reactor when control rods are removed leaving voids. This was done with two different configurations. Also, a value of ν was calculated for a situation where the voids distributed throughout the lattice would be filled with graphite to obtain a comparison of voids to the graphite-filled situation. This was done by extrapolation of the measured buckling curve to the appropriate fuel-to-moderator ratio. These values of the material buckling calculated using the measured ν for the two cases of the voided channels are probably not valid since there are not enough repeating cells in this type of lattice, and the effects of neutron streaming are involved and were not investigated. However, for purposes of comparison to the fully loaded lattice, to determine the effects of voids, these apparent bucklings have been determined using $B^2 = \mu_x^2 + \mu_y^2 - \nu^2$. The values of ν and B^2 are listed in Table V.

TABLE V
B^2 AND ν IN 16-IN. LATTICE WITH VOIDED FUEL CHANNELS

Lattice Configuration	ν (m^{-1})	B^2 (m^{-2})
36-element 16-in. lattice	1.241 ± 0.002	5.50 ± 0.07
A* 30 elements, 6 voids in 16-in. lattice	1.250 ± 0.004	5.46
B* 30 elements, 6 voids in 16-in. lattice	1.204 ± 0.004	5.65
Extrapolated, 30-element, void filled with graphite	1.11	5.88

*Location of voids are shown in Figure 9.

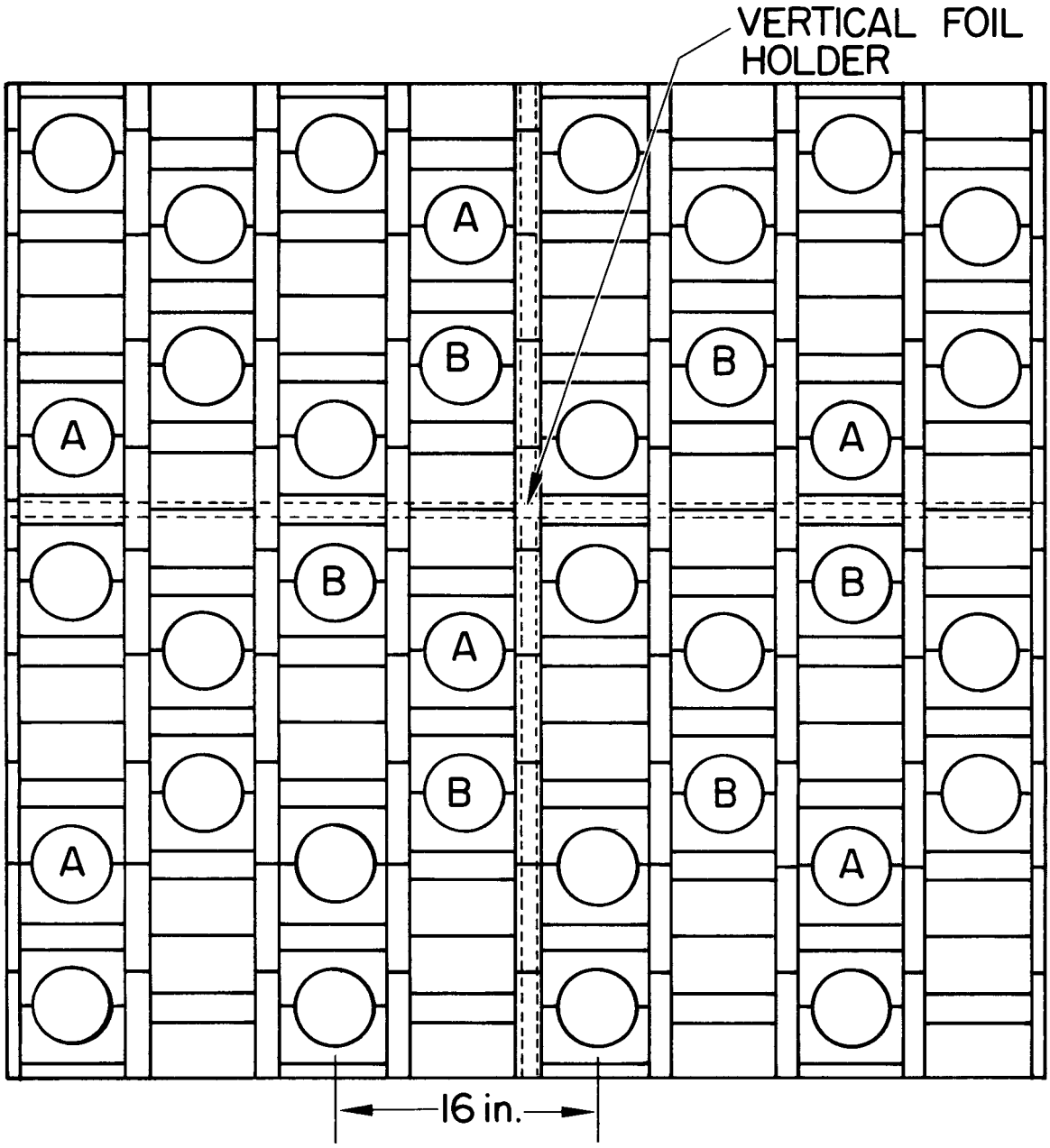

Figure 9. Location of Voided Fuel Channels (Locations marked A and B show positions of voided channels.)

VI. NEUTRON FLUX DISTRIBUTIONS WITHIN A LATTICE CELL

The three hexagonal lattices were studied to determine the neutron flux distributions within lattice cells. For these three lattice spacings a unit cell containing a fuel element of 19 rods, 3-1/2 w/o enriched U - 10 w/o Mo as shown in Figure 10 was studied. Using the 16-in. hexagonal lattice, an 18-rod fuel element of the same fuel composition, a 19-rod, 2.78 w/o enriched U - 10 w/o Mo fuel element, and a UC, 12-rod fuel cluster were studied in a unit cell. Also the 19-rod 3-1/2 w/o enriched U - 10 w/o Mo fuel element was studied in the 16-in. hexagonal lattice where it was surrounded by a zirconium tube to mockup the moderator cladding present in the actual reactor. See Figure 11 for a description of this cell. In all cases the lattice cell of interest was centrally located with the remainder of the lattice being loaded with 3-1/2 w/o enriched, 19-rod, U - 10 Mo fuel clusters.

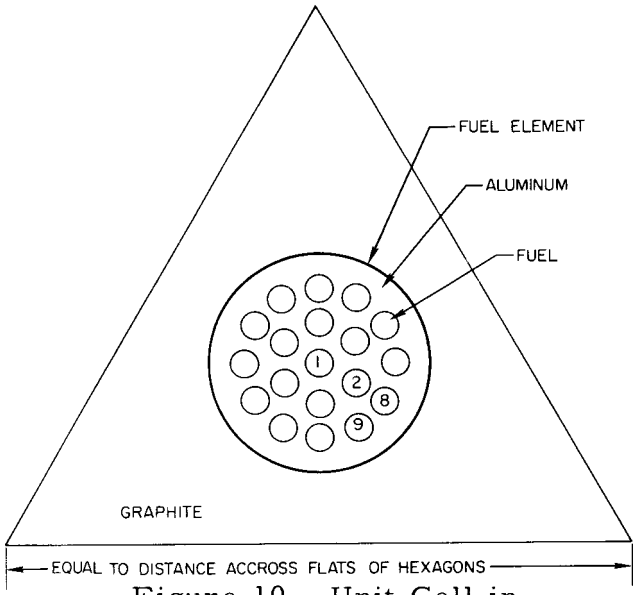

Figure 10. Unit Cell in Hexagonal Lattices

The lattice cell was taken as an equilateral triangle containing the fuel element as shown in Figure 10. Provisions were made in a lattice cell to allow for the placement of the small dysprosium oxide detector foils. Figure 12 shows a horizontal cross section of a typical cell with the locations provided for foil measurements. Measurements were also made in the neighboring cells to check the results of similar points in different cells. Detector foils were placed in the graphite, aluminum, and fuel where the foils were exposed both bare and cadmium covered to allow for the determination of the relative thermal neutron flux distributions. The fuel element of interest was placed in the geometric center of the lattice in the 16-in. and 13-in. lattices. In the 19-in. lattice, the center of a hexagon formed by the fuel elements was at the geometric center of the lattice.

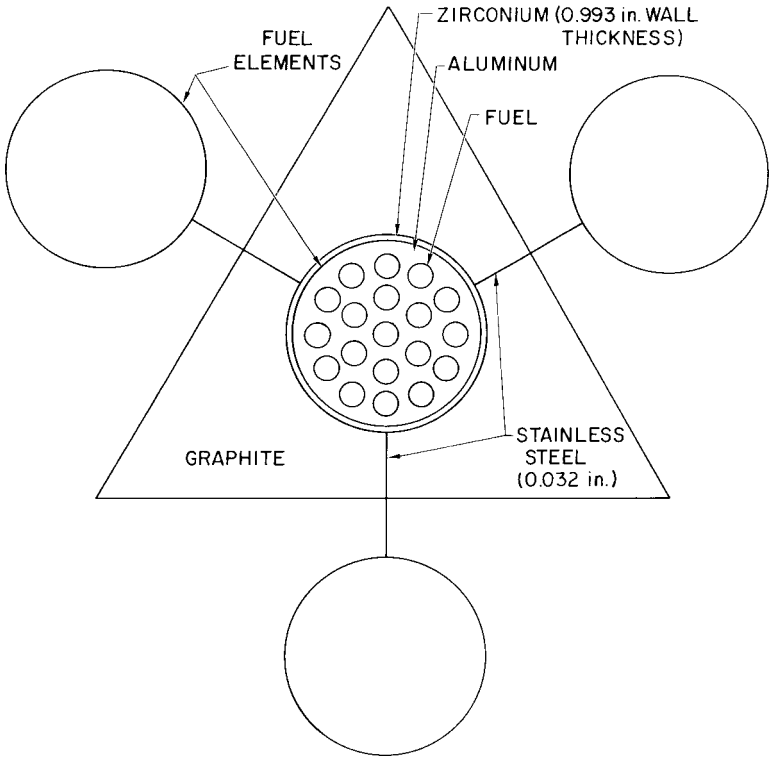

Figure 11. Unit Cell in 16-in. Hexagonal Lattice With Stainless Steel and Zirconium Present

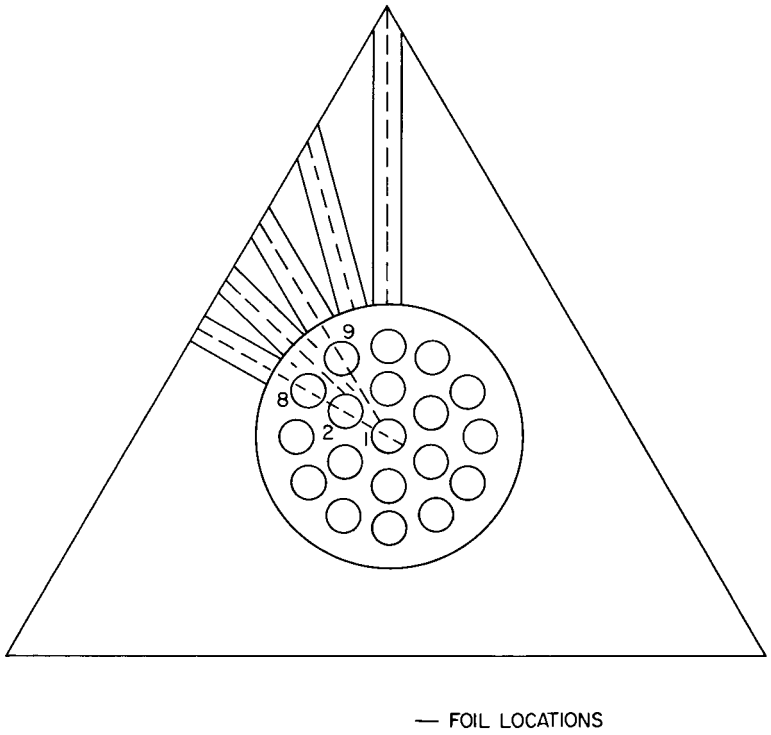

Figure 12. Foil Locations Available Within a Unit Cell

Graphs are included to show typical results for the 19-rod, 3-1/2 w/o U - 10 w/o Mo fuel element in the 16-in. lattice. The different arrangements studied were:

a) 3.448 w/o enriched U - 10 Mo, 19-rod fuel element in 13-in. lattice.

b) 3.448 w/o enriched U - 10 Mo, 19-rod fuel element in 16-in. lattice.

c) 3.448 w/o enriched U - 10 Mo, 18-rod* fuel element in 16-in. lattice.

d) 3.448 w/o enriched U - 10 Mo, 19-rod fuel element in 16-in. lattice with stainless steel and zirconium.†

e) 2.78 w/o enriched U - 10 Mo, 19-rod fuel element in 16-in. lattice.

f) 3.448 w/o enriched U - 10 Mo, 19-rod fuel element in 19-in. lattice.

g) 3.448 w/o enriched U - 4.95 C, 12-rod fuel element in 16-in. lattice.§

In the U - 10 w/o Mo fuel, measurements were made across the diameters of the fuel rods. Figure 13 shows two slotted fuel slugs with inserts for cadmium-covered and bare foil measurements. The bare foil measurements were made with 0.0003-in. aluminum wrappings to eliminate any possible fission products which might contribute to the counting rate. The cadmium-covered foils were contained in 0.020-in. -thick cadmium boxes. For the central rod where the distribution was symmetrical about the rod axis within the accuracy of the measurements, flux measurements along one fuel rod diameter sufficed. For the inner and outer rings of fuel rods where the distributions were not axially symmetrical, a two-dimensional survey of the flux in these rods was obtained by making diametrical flux traverses at angles of 0°, 45°, and 90° to a line through the center of the fuel rod to the center of the cell. The locations of these measurements can be seen in Figure 12. By studying the four fuel rods marked 1, 2, 8, and 9 in Figure 15, the average fluxes for the 19 rods of the element are obtained by use of the physical symmetry present. Typical data are shown in Figure 15. The average relative thermal neutron flux in the various fuel rods for the different situations studied was determined by graphical integration of these graphs.

*The 18-rod element is the same as the 19-rod element except that the central fuel rod has been removed, and a void is left in its place.

†Figure 11 gives a detailed description of the lattice cell with stainless steel and zirconium present.

§Figure 14 gives a detailed description of this lattice cell.

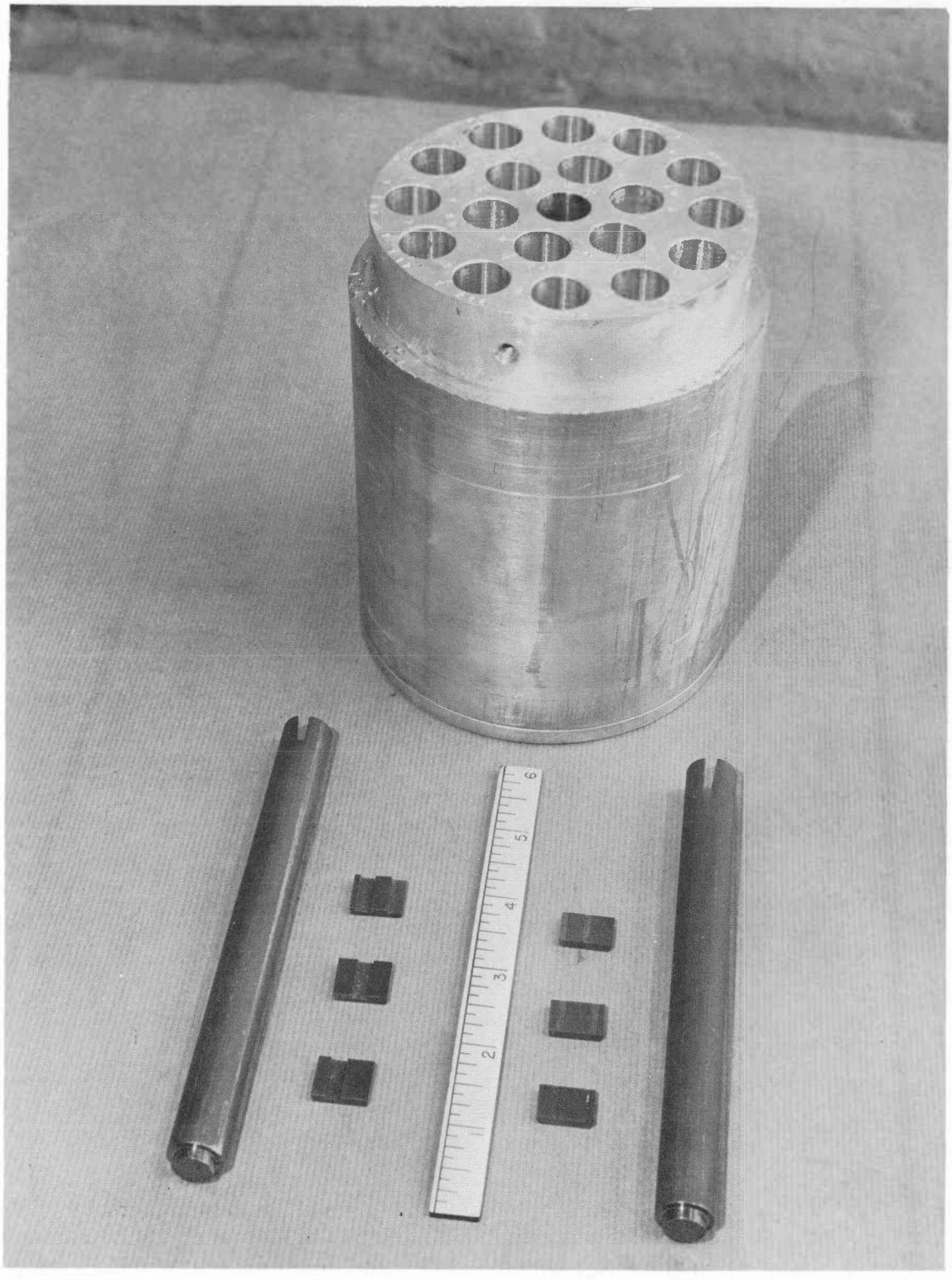

Figure 13. Fuel Slugs With Inserts for Detector Foils and 6-in. Aluminum Fuel Holder Section

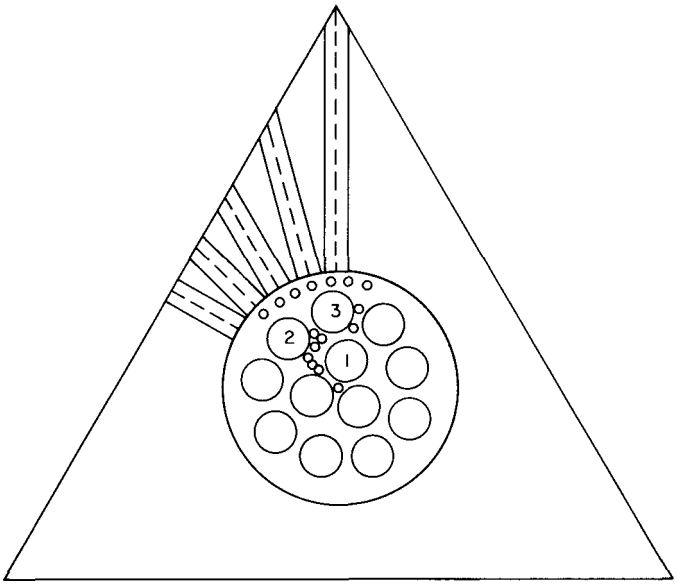

Figure 14. Uranium Carbide Fuel Element Within a Lattice Cell

Because of the difficulty in machining uranium carbide, a different technique was used to determine the relative average thermal neutron flux in that fuel cluster. In order to determine the average relative thermal neutron flux in each carbide fuel rod circular detector foils, with the same diameter as the fuel slugs, were exposed both bare and cadmium covered in the fuel rods. Three of the fuel rods referred to as 1, 2, and 3 as shown in Figure 6, which represent the entire fuel element through symmetry, were studied. The placement of these foils in the fuel with and without cadmium covers can be seen in Figure 16.

The foils used to determine the relative neutron fluxes in the fuel were 18.7 w/o U with an enrichment of 93.37 w/o U^{235}, the remainder being aluminum. The fission product activities of these foils were determined by counting the gamma rays of energy above 0.5 Mev. These measurements will be discussed in more detail in Sections VIII and IX. These results were normalized to the results from the dysprosium oxide foil measurements in the graphite and aluminum by making measurements with both type foils in the graphite.

The method of determining the relative thermal neutron flux in the UC fuel described above was compared to the small foil technique, where foils are placed along several diameters, also described above. This comparison was made in a 19-rod U-Mo fuel element. The results were in agreement to within ±0.2% for each rod.

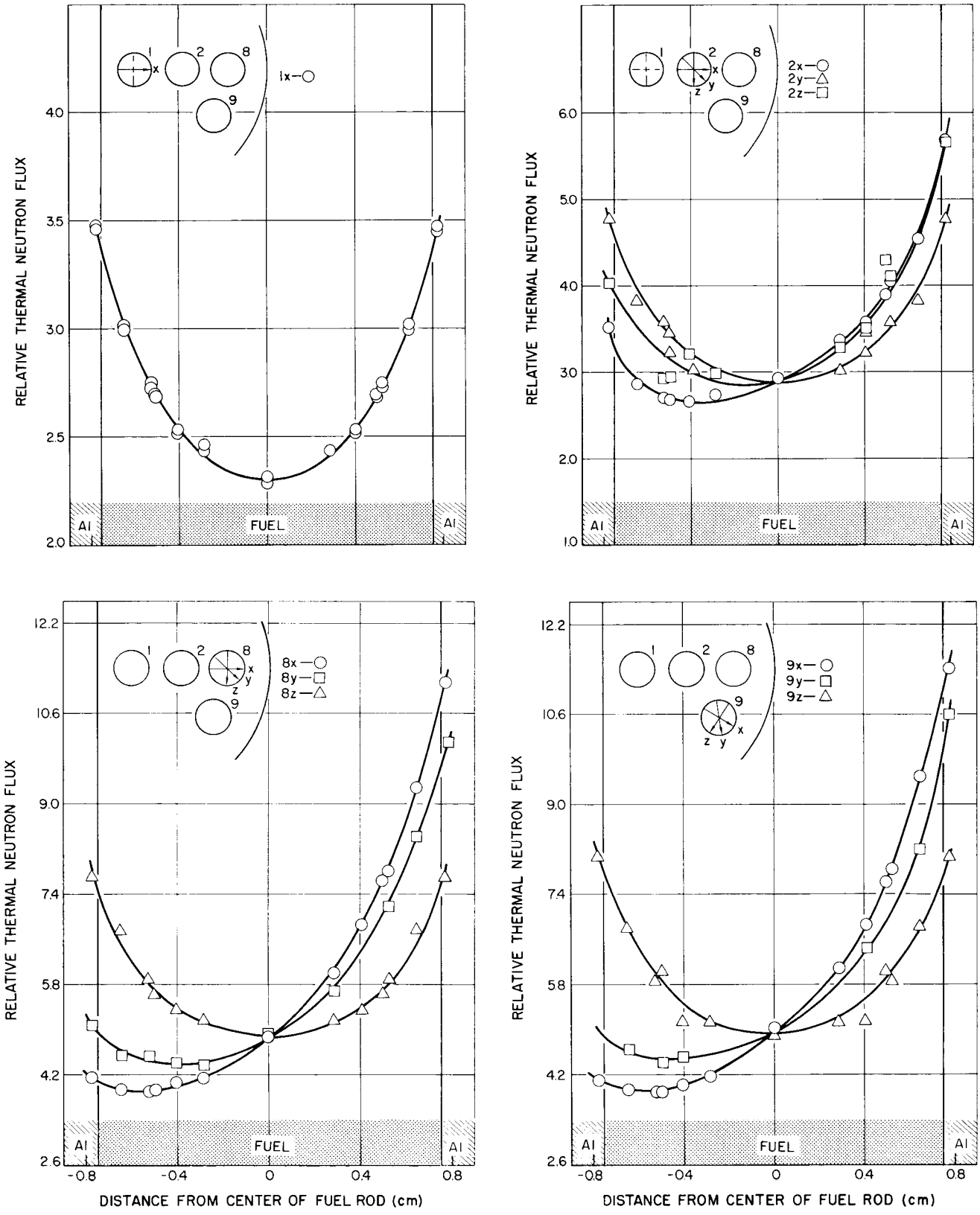

Figure 15. Thermal Neutron Flux Distributions in Fuel Rods for the 19-Rod, 3-1/2 w/o Enriched U - 10 Mo Fuel Element in the 16-in. Lattice

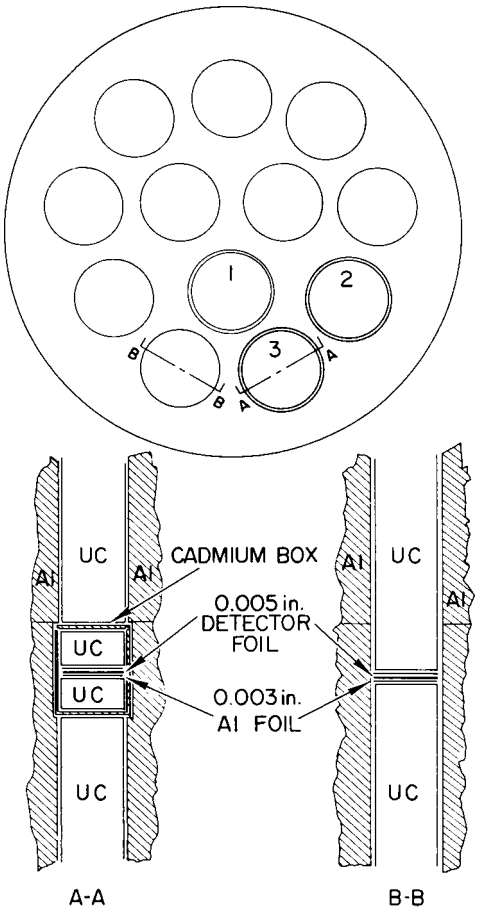

Figure 16. View of the UC Fuel Element Arrangement for Obtaining Foil Activations

Several of the aluminum fuel holders were designed so they could be split at the 21-in. and 30-in. levels to allow for the removal of a 6-in. section which contained the detector foils for the neutron distribution measurements. One 6-in. section of aluminum fuel holder can be seen in Figure 17. Figure 17 shows an aluminum fuel holder with the provision for determining the neutron flux distribution within the aluminum. Measurements were also made at the surfaces between the aluminum and the fuel rods. The holes shown in Figure 17 were either filled with aluminum plugs containing detector foils or with solid aluminum plugs. The solid plugs were used when measurements were not required in that material. By measuring the thermal neutron flux distributions in a 30° section of the aluminum fuel holder for the 19-rod element and a 60° section for the UC element, the thermal neutron flux in the entire aluminum holder was represented through symmetry. The measured value of the relative thermal neutron flux was plotted for each measured point in the aluminum to make a contour mapping of the relative fluxes in the aluminum. Figure 18 shows a typical result of this work. By graphically integrating the small areas, using a compensating polar planimeter, and finding the average relative fluxes, the average relative thermal neutron flux in the aluminum was determined.

To obtain the relative average thermal neutron flux in the graphite, neutron flux distribution measurements were made in the locations shown in Figure 12. Holes, 5/8-in. in diameter, were drilled in the graphite, in the lattice cell being studied, to accept the graphite foil holders. The graphite foil holders had provisions for foils to be placed at 1-cm intervals. The equilateral triangle which makes up a lattice cell can be divided into 6 symmetrical 30° - 60° - 90° triangles with the 60° vertex in the center of the cell. By determining the average relative thermal neutron flux in one of these right triangles, the average flux

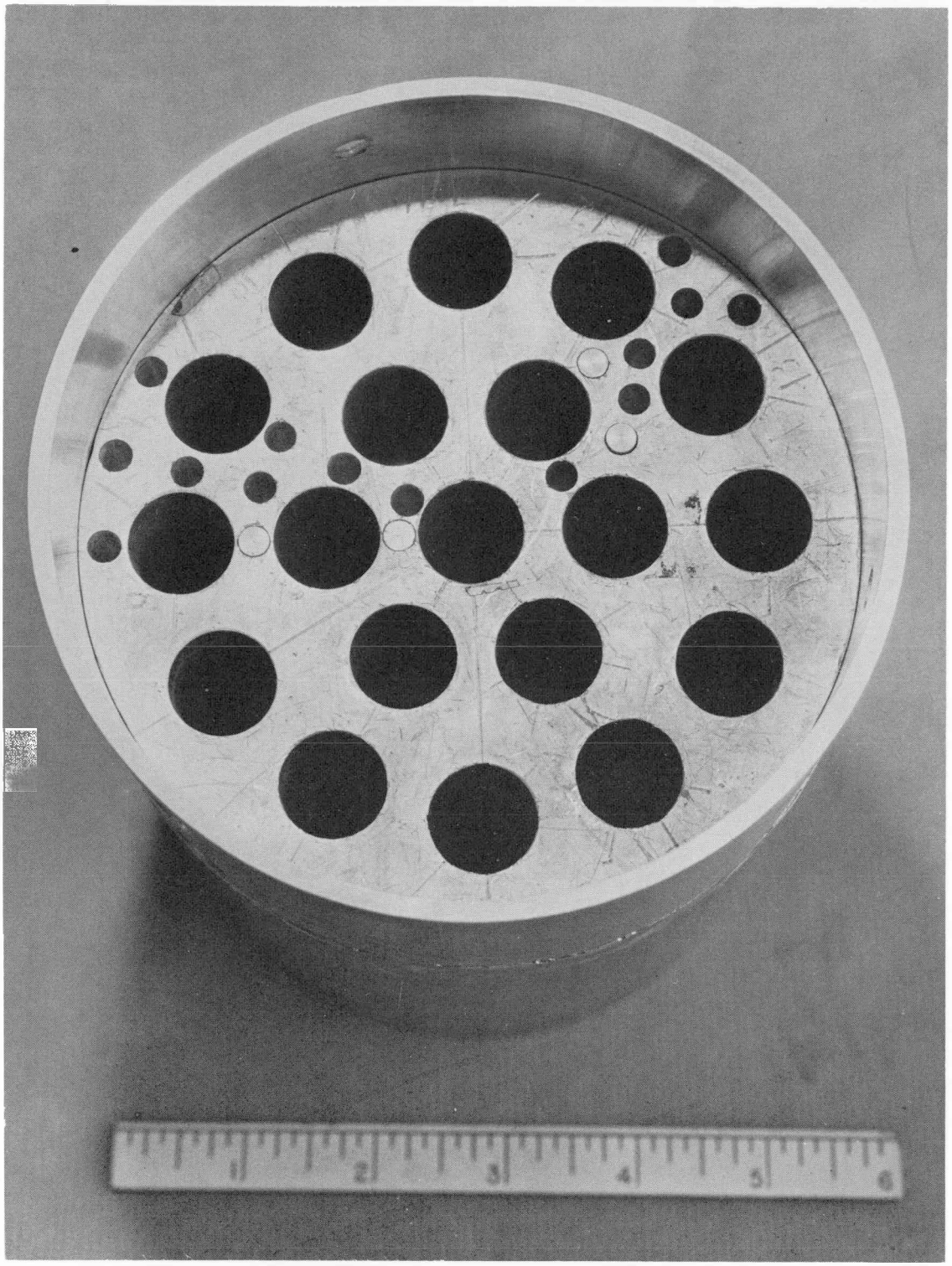

Figure 17. Six-Inch Section of Aluminum Fuel Holder With Provisions for Measurements in the Aluminum

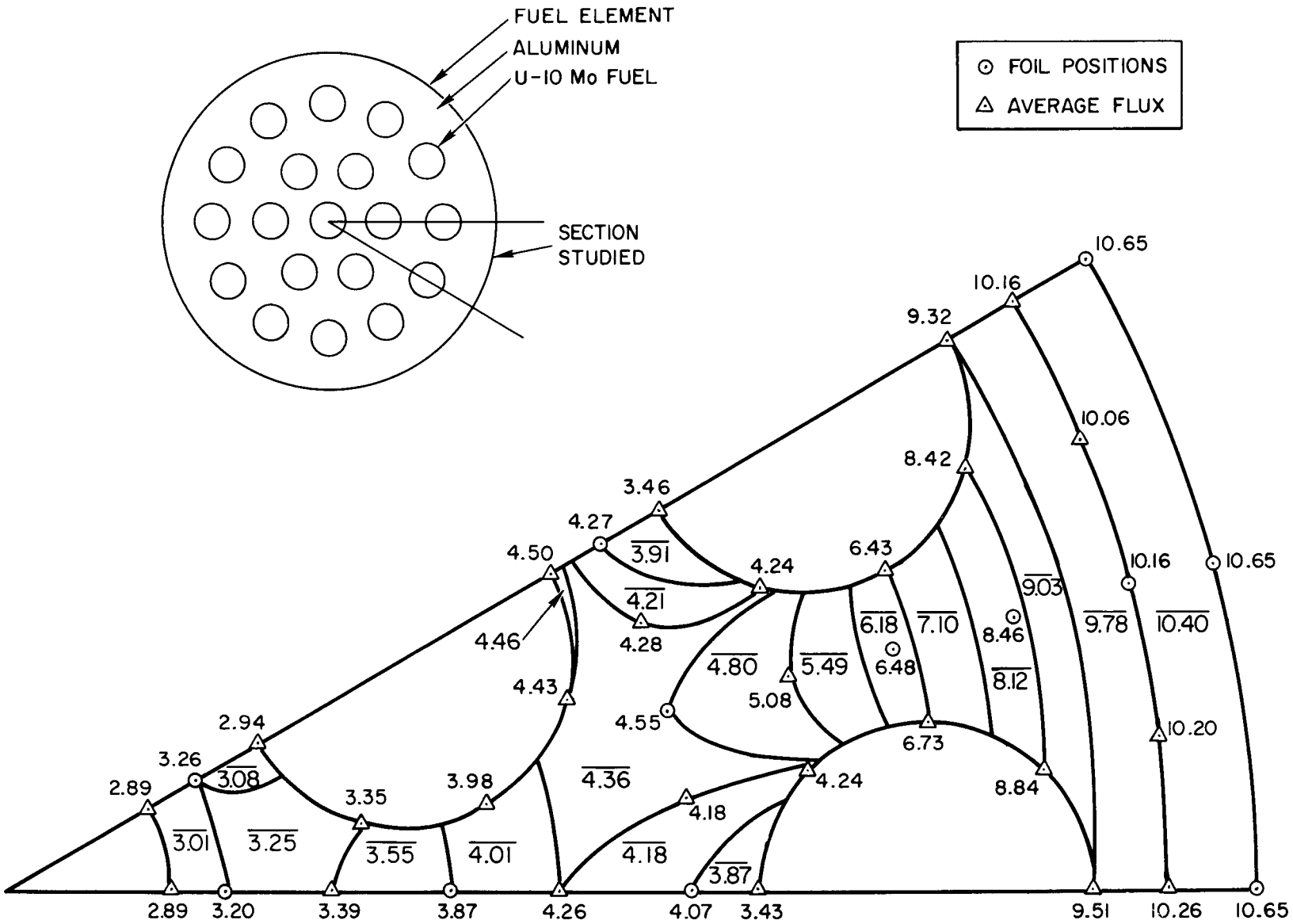

Figure 18. Section of Aluminum Fuel Holder Showing Relative Average Thermal Neutron Fluxes (19-rod, 3-1/2 w/o Enriched U - 10 w/o Mo Fuel Element in the 16-in. Hexagonal Lattice With SS and Zr)

in the graphite is known. To determine the average flux in the 30° - 60° - 90° triangles, flux plots were made at 15° intervals through the 60° angle. A typical graph showing this plot can be seen in Figure 19. From this plot the average relative thermal neutron flux in the graphite was determined by graphical integration. Figure 20 shows the relative epithermal neutron flux in a lattice cell and cadmium ratios.

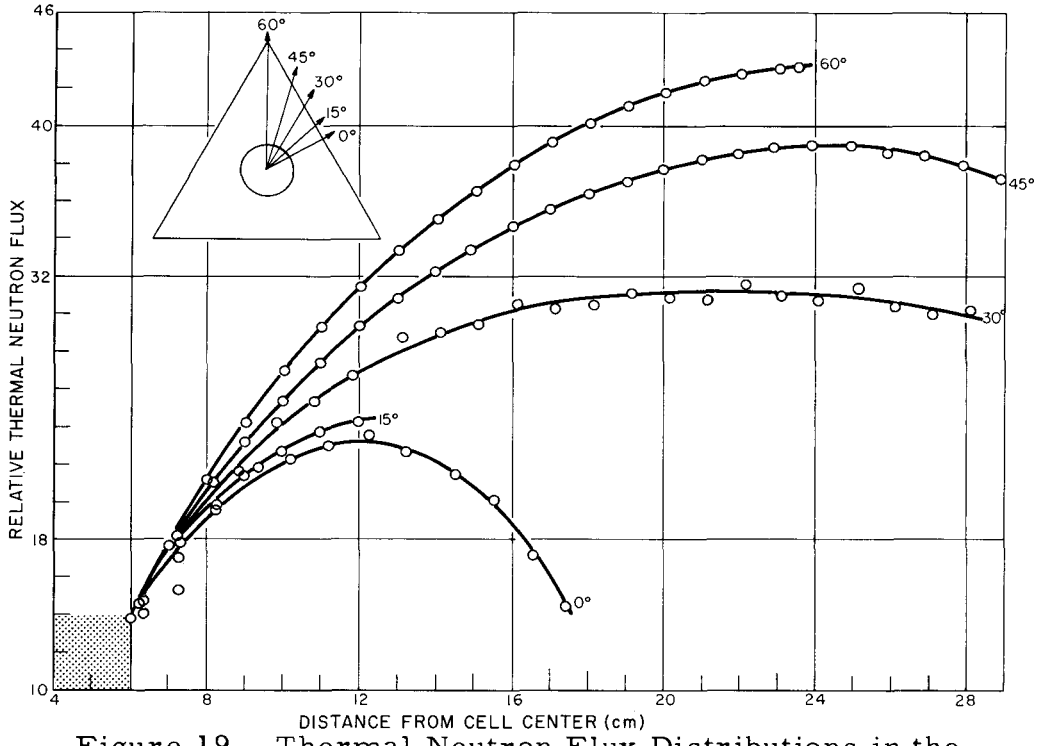

Figure 19. Thermal Neutron Flux Distributions in the Graphite for the 19-rod, 3-1/2 w/o Enriched U - 10 w/o Mo Fuel Element in the 16-in. Lattice

For the one case where the fuel element was surrounded by stainless steel and zirconium, Figure 11, the relative average thermal neutron fluxes for these materials were determined by placing detector foils along their surfaces and averaging the measured values obtained.

Table VI gives a summary of the relative average thermal neutron flux determined for each material of each cell studied. The results in Table VI for each case have been normalized so the average relative thermal neutron flux in a fuel rod of the outer ring of fuel rods is equal to one.

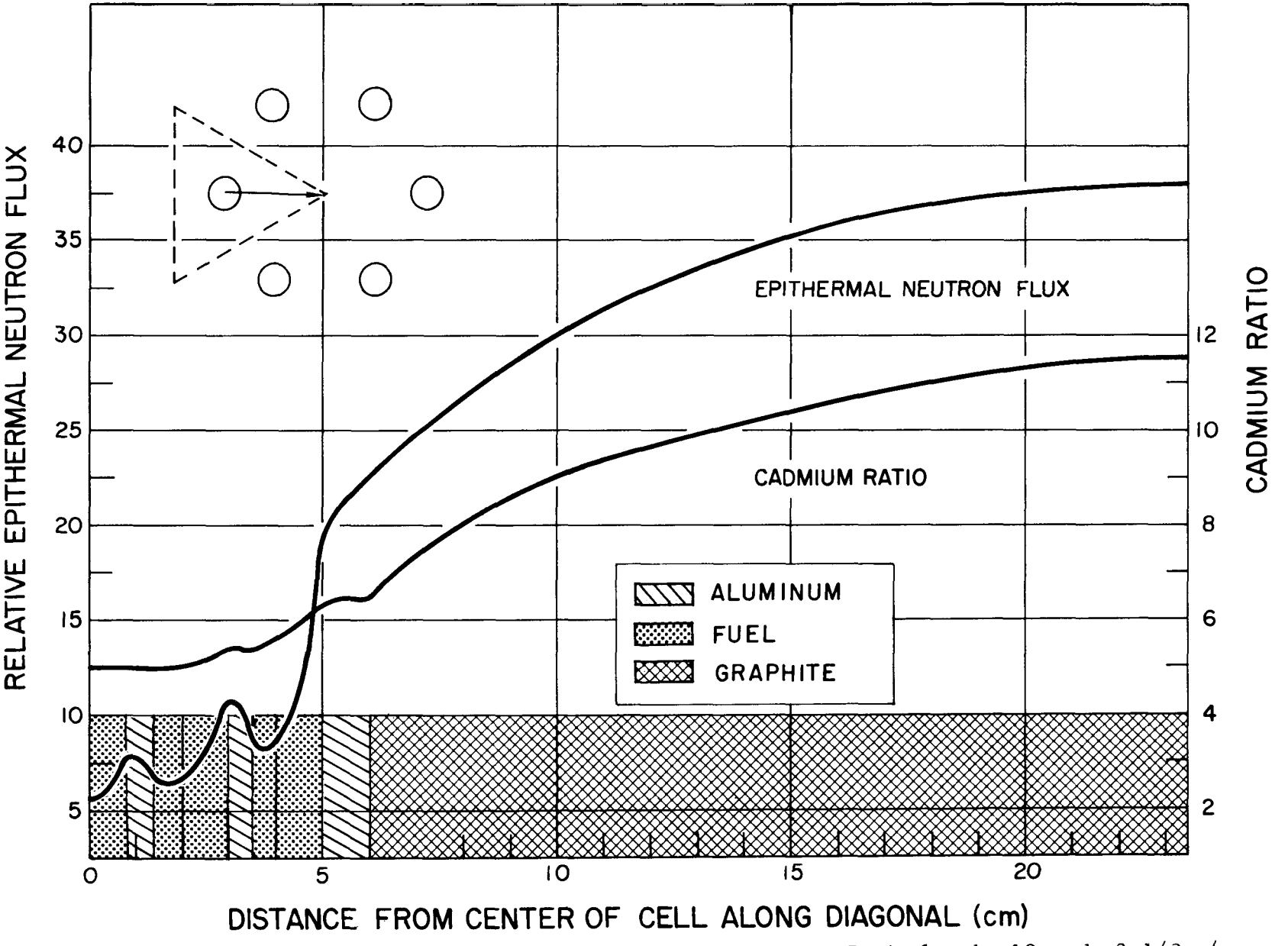

Figure 20. Epithermal Neutron Flux Distribution and Cadmium Ratio for the 19-rod, 3-1/2 w/o Enriched U - 10 w/o Mo Fuel Element in the 16-in. Hexagonal Lattice

TABLE VI

RELATIVE AVERAGE THERMAL NEUTRON FLUX

Cell Studied	Fuel					Avg.	Graphite	Aluminum	SS	Zr
	Rod 1	Rod 2	Rod 3	Rod 8	Rod 9					
3.448 w/o enriched U - 10 w/o Mo, 19-rod fuel element in 13-in. lattice	0.510 ±0.003	0.606 ±0.016		0.991 ±0.012	1.009 ±0.009	0.850 ±0.006	3.596 ±0.052	1.467 ±0.012		
3.448 w/o enriched U - 10 w/o Mo, 19-rod fuel element in 16-in. lattice	0.464 ±0.003	0.584 ±0.012		1.000 ±0.008	1.000 ±0.007	0.840 ±0.004	4.670 ±0.060	1.516 ±0.009		
3.448 w/o enriched U - 10 w/o Mo, 18-rod fuel element in 16-in. lattice	void	0.605 ±0.009		1.000 ±0.010	1.000 ±0.010	0.868 ±0.005	4.609 ±0.060	1.496 ±0.012		
3.448 w/o enriched U - 10 w/o Mo, 19-rod fuel element in 16-in. lattice with SS and Zr	0.475 ±0.004	0.608 ±0.006		1.000 ±0.011	1.000 ±0.011	0.848 ±0.005	4.833 ±0.072	1.399 ±0.012	3.381 ±0.039	2.265 ±0.014
2.78 w/o enriched U - 10 w/o Mo, 19-rod fuel element in 16-in. lattice	0.522 ±0.004	0.625 ±0.010		0.994 ±0.009	1.006 ±0.010	0.856 ±0.005	4.113 ±0.052	1.438 ±0.010		
3.448 w/o enriched U - 10 w/o Mo, 19-rod fuel element in 19-in. lattice	0.441 ±0.005	0.525 ±0.012		1.000 ±0.012	1.000 ±0.013	0.821 ±0.006	5.653 ±0.076	1.651 ±0.011		
3.448 w/o enriched U - 4.95 w/o C, 12-rod fuel element in 16-in. lattice	0.607 ±0.040	0.956 ±0.050	1.000 ±0.025			0.891 ±0.032	3.439 ±0.051	1.245 ±0.015		

VII. THERMAL UTILIZATION

In order to determine the thermal utilization, given by

$$f = \frac{\Sigma_{a\,(fuel)}\, V_{(fuel)}\, \overline{\phi}_{(fuel)}}{\Sigma_{a_i}\, V_i\, \overline{\phi}_i}$$

where Σ_{a_i} is the macroscopic absorption cross section, i^{th} component of a unit cell, $\overline{\phi}_i$ is the corresponding average thermal neutron flux, and V_i is the corresponding volume fraction. The relative average thermal neutron flux was measured for each material in the unit cell. The volumes are taken from the dimensions of the materials in the unit cell studied. The microscopic cross sections and densities are given in Section II, Table II. The values used for the macroscopic thermal neutron absorption cross sections are given in Table VII. These results have been used to determine the thermal utilization of each lattice. The values of thermal utilization obtained for the various lattice cells studied are given in Table VIII.

TABLE VIII

RESULTS OF THERMAL UTILIZATION

Fuel Element	Lattice	f
3.448 w/o enriched U - 10 w/o Mo, 19-rod	13-in.	0.919 ± 0.013
3.448 w/o enriched U - 10 w/o Mo, 19-rod	16-in.	0.885 ± 0.009
3.448 w/o enriched U - 10 w/o Mo, 19-rod	19-in.	0.832 ± 0.012
3.448 w/o enriched U - 10 w/o Mo, 18-rod	16-in.	0.884 ± 0.011
2.78 w/o enriched U - 10 w/o Mo, 19-rod	16-in.	0.876 ± 0.010
3.448 w/o enriched U - 10 w/o Mo, 19-rod with SS and Zr	16-in.	0.859 ± 0.010
3.448 w/o enriched UC, 12-rod	16-in.	0.906 ± 0.018

TABLE VII

VOLUMES AND MACROSCOPIC THERMAL NEUTRON CROSS SECTIONS

Cell Studied	Volume (cm^3)					Σ_a (cm^{-1})				
	Fuel	Graphite	Aluminum	SS	Zr	Fuel	Graphite	Aluminum	SS	Zr
3.448 w/o enriched U - 10 w/o Mo, 19-rod fuel element in 13-in. lattice	33.74 ±0.13	357.80 ±0.29	78.49 ±0.60			0.9245 ±0.0065	0.5127×10^{-3} $\pm 0.0302 \times 10^{-3}$	0.01461 ±0.00035		
3.448 w/o enriched U - 10 w/o Mo, 19-rod fuel element in 16-in. lattice	33.74 ±0.13	600.84 ±0.29	78.49 ±0.60			0.9245 ±0.0065	0.5997×10^{-3} $\pm 0.0299 \times 10^{-3}$	0.01461 ±0.00035		
3.448 w/o enriched U - 10 w/o Mo, 18-rod fuel element in 16-in. lattice	31.96 ±0.12	600.84 ±0.29	78.49 ±0.60			0.9245 ±0.0065	0.5997×10^{-3} $\pm 0.0299 \times 10^{-3}$	0.01461 ±0.00035		
3.448 w/o enriched U - 10 w/o Mo, 19-rod fuel element in 16-in. lattice with SS and Zr	33.74 ±0.13	600.84 ±0.29	67.25 ±0.56	1.390 ±0.020	9.404 ±0.094	0.9245 ±0.0065	0.5997×10^{-3} $\pm 0.0299 \times 10^{-3}$	0.01461 ±0.00035	0.230 ±0.006	8.154×10^{-3} $\pm 0.179 \times 10^{-3}$
2.78 w/o enriched U - 10 w/o Mo, 19-rod fuel element in 16-in. lattice	33.74 ±0.13	600.84 ±0.29	78.49 ±0.60			0.7679 ±0.0056	0.5997×10^{-3} $\pm 0.0299 \times 10^{-3}$	0.01461 ±0.00035		
3.448 w/o enriched U - 10 w/o Mo, 19-rod fuel element in 19-in. lattice	33.74 ±0.13	894.21 ±0.29	78.49 ±0.60			0.9245 ±0.0065	0.6494×10^{-3} $\pm 0.0377 \times 10^{-3}$	0.01461 ±0.00035		
3.448 w/o enriched U 4.95 w/o C, 12-rod fuel element in 16-in. lattice	38.72 ±0.18	600.84 ±0.29	74.14 ±0.61			0.7319 ±0.0042	0.5997×10^{-3} $\pm 0.0299 \times 10^{-3}$	0.01461 ±0.00035		

VIII. RATIO OF RESONANCE TO THERMAL CAPTURE PROBABILITIES IN U^{238}

Measurements have been made to determine the ratio of the resonance capture probability to the thermal capture probability in U^{238}. The method used[5] to determine this ratio is briefly described below. Uranium-238 detector foils are exposed in various positions in the fuel rods, and the activity resulting from the U^{238} (n, ν) reaction in the fuel is measured. The U^{238} (n, ν) reaction proceeds as follows:

$$_{92}U^{238} + {}_{o}N^{1} \longrightarrow {}_{92}U^{239} \xrightarrow[23\ \text{min}]{\beta,\ \nu} {}_{32}N_{p}{}^{239} \xrightarrow[2.346\ \text{days}]{\beta,\ \nu} {}_{94}Pu^{239} \xrightarrow{\nu} .$$

The 103-kev internal conversion X-ray activity from plutonium which follows the neptunium activity is measured. This activity is measured for both bare and cadmium covered foils. The ratio, r_p, of the resonance capture probability to the thermal capture probability in U^{238} is given by

$$r_p = \frac{\bar{A}_{49}^{cd}}{\bar{A}_{49}^{b} - \bar{A}_{49}^{cd}} \quad .$$

Where the bars indicate average activities for the fuel in the fuel element, cd and b refer to cadmium-covered and bare foils activities respectively, and 49 refers to the plutonium X-ray activity. Measurements were made in the three hexagonal lattices in a centrally located 19-rod fuel element and in the UC fuel element in the 16-in. lattice.

Both bare and cadmium-covered 20-fold depleted uranium foils were irradiated in enough positions in the fuel element that the activities of these could be averaged over a unit volume of the fuel. The fuel rod positions studied and the averaging process for the fuel element is the same as that discussed in Section VI. Circular foils having the same diameter as the fuel rods were exposed. By counting these, the average activities for the various fuel rods were obtained directly. By proper mass and run normalization and averaging over the fuel element, the relative activities for the two type foils both bare and cadmium-covered were obtained. Figures 16 and 21 show the arrangements used to obtain bare and cadmium-covered results. Figure 16 shows the placement of the foils in the

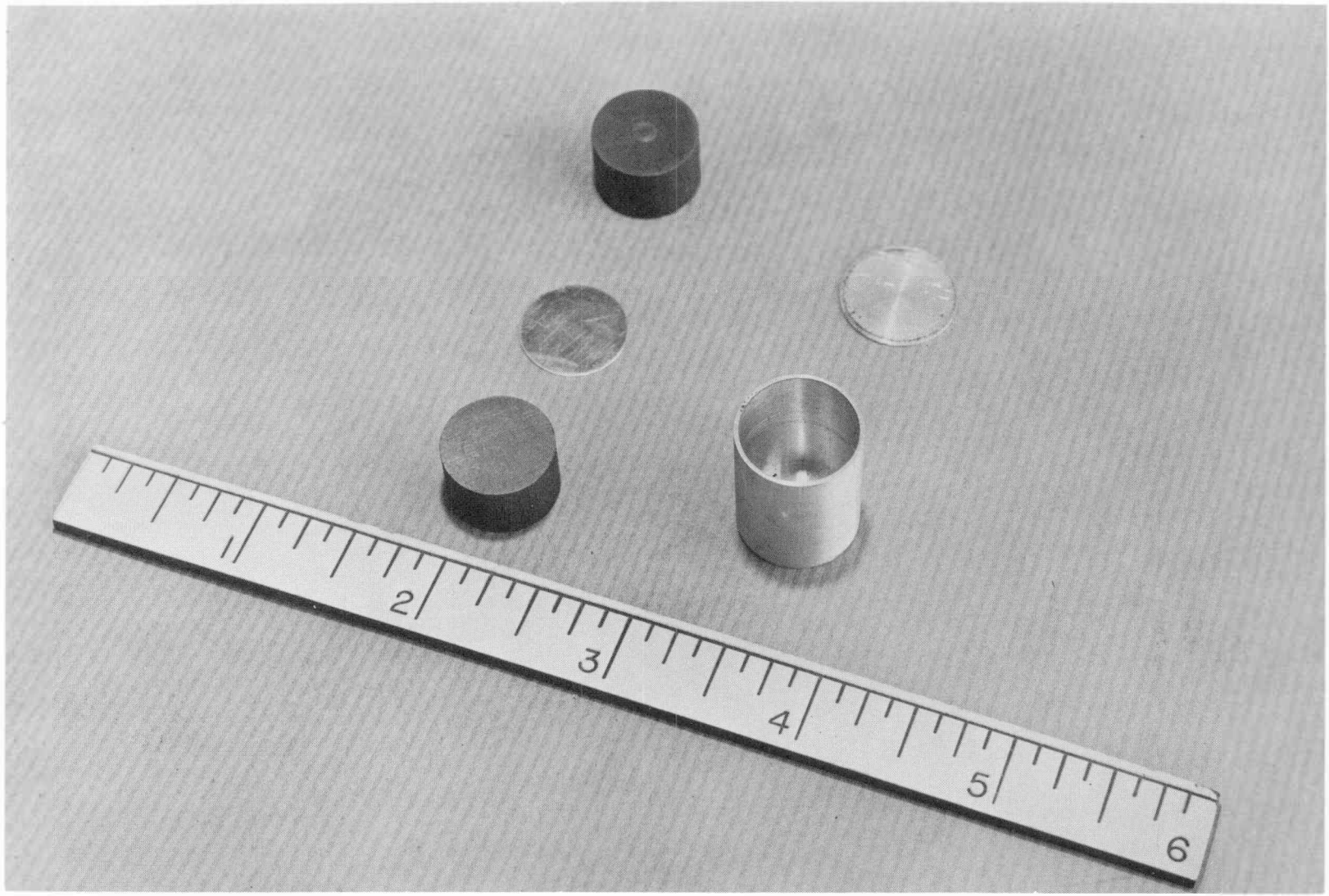

Figure 21. Uranium Molybdenum Discs, Detector Foil, and Cadmium Box

fuel rods. The fuel rod discs on each side of the detector foils were carefully machined to assure flat smooth surfaces to prevent streaming. The foils were covered by 0.0003-in. aluminum foil to prevent fission product contamination from the fuel slugs upon irradiation. To obtain the cadmium-covered results, the foils and the fuel in the immediate neighborhood were surrounded by cylindrical cadmium boxes as shown in the figures. The flux depression of fast neutrons due to the cadmium boxes has been investigated elsewhere.[6] It has been found that this effect is negligible.

The depleted uranium foils available for these experiments contained about 360 ppm U^{235}, 20-fold depleted. In counting the buildup of plutonium, the contribution due to fission product decay gamma-rays and uranium X-rays appears in the energy region of 103-kev. The method of correcting for the undesired fission product activities was obtained from references 7 and 8. The method used is briefly described below.

Bare and cadmium-covered natural and depleted uranium foils are counted in the 103-kev window of the counters. The counters and counting techniques were discussed earlier. These activities may be represented by the following equations:

$$A_D^b = A_{49}^b + A_{28}^b + dA_{25}^b$$

$$A_N^b = A_{49}^b + A_{28}^b + A_{25}^b$$

$$A_D^{cd} = A_{49}^{cd} + A_{28}^{cd} + dA_{25}^{cd}$$

$$A_N^{cd} = A_{49}^{cd} + A_{28}^{cd} + A_{25}^{cd}$$

In the equations the superscripts and subscripts refer to the following:

b to bare foils,
cd to cadmium-covered foils,
D to depleted foils,
49 to 103-kev plutonium X-ray,
d to depletion factor (U^{235} depleted foil/U^{235} natural foil),
N to natural uranium foil,

28 to γ-rays from U^{238} fission product feeding into the 103-kev window due to attenuation processes, and

25 to γ-rays from U^{235} fission product feeding into the 103-kev window due to attenuation processes.

The activities A_{49}^b and A_{49}^c are required for determining r_p from

$$r_p = \frac{A_{49}^c}{A_{49}^b - A_{49}^c} \quad .$$

From the first two equations above, the ratio

$$r^b = \frac{A_D^b - A_{49}^b}{A_N^b - A_{49}^b} = \frac{A_{28}^b + dA_{25}^b}{A_{28}^b + A_{25}^b}$$

may be formed. The right-hand member of the equation is the ratio of attenuated gamma rays from the depleted uranium foil to those from the natural uranium foil. To determine the ratio r^b, the counting equipment was set with a bias of 0.5 Mev, and the foils were counted integrally giving the following activities

$$^iA_D^b = {}^iA_{28}^b + d^iA_{25}^b \quad ,$$

$$^iA_N^b = {}^iA_{28}^b + {}^iA_{25}^b \quad ,$$

where the superscript i refers to counting having been done "integrally." A ratio

$$^ir^b = \frac{^iA_{28}^b + d^iA_{25}^b}{^iA_{28}^b + {}^iA_{25}^b}$$

may be formed. If one assumes

$$r^b = {}^ir^b \quad ,$$

TABLE IX

MEASURED RELATIVE 103-kev ACTIVITIES AND RELATIVE FISSION PRODUCT ACTIVITIES IN THE U - 10 Mo FUEL

Detector Foil	Lattice	Fuel	103-kev Activities (A)						Fission Product Activities ($\dot{A}$)					
			Rod 1	Rod 2	Rod 3	Rod 8	Rod 9	Avg. Fuel ($\bar{A}$)	Rod 1	Rod 2	Rod 3	Rod 8	Rod 9	Avg. Fuel ($\bar{\dot{A}}$)
Natural U	13-in.	U - 10 Mo	6394	6662		8090	8667	7732 ± 77	23190	25416		31521	31954	29291 ± 237
Depleted U	13-in.	U - 10 Mo	6050	6395		8037	8014	7407 ± 63	7736	7528		7777	7443	7591 ± 83
Natural U, Cd-covered	13-in.	U - 10 Mo	5299	5506		7219	6894	6474 ± 75	13718	14384		15297	15092	14861 ± 102
Depleted U, Cd-covered	13-in.	U - 10 Mo	5291	5726		6968	7011	6501 ± 42	6645	6148		5580	5829	5894 ± 47
Natural U	16-in.	U - 10 Mo	5667	6295		7757	7771	7190 ± 83	33635	37428		50518	51041	45661 ± 361
Depleted U	16-in.	U - 10 Mo	5305	5711		7496	7412	6790 ± 52	13155	13680		14233	14302	14023 ± 98
Natural U, Cd-covered	16-in.	U - 10 Mo				6309	6281		16952	17309		17561	17472	17421 ± 87
Depleted U, Cd-covered	16-in.	U - 10 Mo	4613	4928		6164	6139	5684 ± 43	10316	10209		8947	8789	9368 ± 121
Natural U	19-in.	U - 10 Mo	4127	4461		5928	5867	5351 ± 52	10155	10829		15091	15416	13588 ± 101
Depleted U	19-in.	U - 10 Mo	4168	4334		5741	5767	5222 ± 37	3879	4036		4431	4282	4230 ± 107
Natural U, Cd-covered	19-in.	U - 10 Mo	3595	3831		4685	4682	4357 ± 33	5247	5255		5143	5259	5231 ± 41
Depleted U, Cd-covered	19-in.	U - 10 Mo	3533	3706		4824	4824	4403 ± 40	3094	3103		2796	2618	2852 ± 58
Natural U	16-in.	UC	3828	4816	5116			4719 ± 71	17051	22091	23040			21305 ± 422
Depleted U	16-in.	UC	3769	4814	4993			4642 ± 68	6412	7342	6938			6908 ± 140
Natural U, Cd-covered	16-in.	UC	3273	3814	3921			3732 ± 63	6991	8759	8757			8317 ± 167
Depleted U, Cd-covered	16-in.	UC	3150	3753	3858			3655 ± 59	5107	4520	4545			4679 ± 92

then the ratio r^b can in effect be measured. This gives the equation:

$$i_r{}^b = \frac{A_D^b - A_{49}^b}{A_N^b - A_{49}^b} \quad ,$$

which one can solve for A_{49}^b. The cadmium-covered activities can be treated similarly to obtain A_{49}^{cd}. From these the ratio r_p is obtained.

The results reported are relative activities. They have all been mass and run normalized and have been corrected for buckling for the lattice in which the measurements were made. The values of the activities measured for the natural and depleted uranium foils both bare and cadmium covered are listed in Table IX. The results are shown for each representative fuel rod for each lattice studied and the average for the fuel is given in each case.

Using the correction discussed, the values of A_{49}^b (Pu^{239} X-ray activity) and A_{49}^{cd} (Pu^{239} X-ray activity for cadmium-covered foils) were obtained. Having these results the ratio

$$r_p = \frac{A_{49}^{cd}}{A_{49}^b - A_{49}^{cd}}$$

was determined. The results for the various lattices are given in Table X.

TABLE X

CORRECTED Pu^{239} X-RAY ACTIVITIES AND RATIOS OF RESONANCE TO THERMAL CAPTURES IN U^{238}

Fuel	Lattices	A_{49}^{cd}	A_{49}^b	r_p
U - 10 Mo	13-in.	6501 ± 42	7407 ± 63	7.17 ± 0.46
U - 10 Mo	16-in.	5627 ± 41	6601 ± 52	5.78 ± 0.32
U - 10 Mo	19-in.	4362 ± 40	5160 ± 37	5.46 ± 0.36
UC	16-in.	3556 ± 64	4608 ± 71	3.38 ± 0.32

The fairly large errors in r_p are due to taking the differences of numbers where the remainder is small in comparison to the numbers themselves. In this case, subtracting measured values with errors of less than 1% gives results with errors of about 6%.

IX. RATIO OF THE U^{238} FISSION PROBABILITY TO THE U^{235} FISSION PROBABILITY

Measurements have been made to determine the ratios of the U^{238} fission probability to the total U^{235} fission probability and the U^{238} fission probability to the thermal U^{235} fission probability, referred to as $r_{\epsilon 1}$ and $r_{\epsilon 2}$, respectively. These measurements have been made using U^{235} alloyed with aluminum and natural uranium detector foils. Measurements have been made for both bare and cadmium-covered foils where the fission product activities were determined by counting the gamma rays above 0.5 Mev energy. These measurements have been made in the U - 10 w/o Mo fuel elements in the 13-, 16-, and 19-in. lattices and in the UC element in the 13- and 16-in. lattices.

The ratios to be determined are given by

$$r_{\epsilon 1} = \frac{i\overline{A}_{28}^{cd}}{i\overline{A}_{25}^{b}} \qquad \text{and} \qquad r_{\epsilon 2} = \frac{i\overline{A}_{28}^{cd}}{i\overline{A}_{25}^{b} - i\overline{A}_{25}^{cd}} \; .$$

In the equation the superscripts and subscripts refer to the following:

i indicates the activities were determined by integral counting above 0.5 Mev,

cd refers to cadmium-covered data,

b refers to total activity data, and

$\overline{A}$ indicates the activities were averaged over the 19 fuel rods in a fuel element.

The activities measured using the natural and enriched uranium detector foils have been corrected to give the results that would be obtained for a fuel sample.

The measuring techniques used to determine the ratio of the U^{238} fissions to the U^{235} fissions involves counting the activities above 0.5 Mev of detector foils. The counting techniques have been discussed. The method used to correct the measured data to apply to the ratios required was suggested in a private communication.[8] The following is a brief description of the method used.

Bare and cadmium-covered enriched uranium alloyed with aluminum and natural uranium foils were counted, after being exposed in the lattice, to determine the relative fission product activities. These activities are represented by

$$ {}^{i}A_{E}^{cd},\ {}^{i}A_{E}^{b},\ {}^{i}A_{N}^{cd},\ \text{and}\ {}^{i}A_{N}^{b} $$

where the N and E refer to natural and enriched foils.

First consider the problem of determining the relative U^{238} fission product activity for a foil of the same U^{238} atom density as the fuel material. The epicadmium fission product activity in a natural uranium foil is given by

$$ {}^{i}A_{N}^{cd} = {}^{i}A_{28}^{cd} + {}^{i}A_{25}^{cd} \quad . $$

The highly enriched uranium alloyed with aluminum foil activities are almost entirely due to the U^{235}. The U^{238} present contributes less than 0.1%, so this part has been neglected. The cadmium-covered activities of these foils are represented by ${}^{i}A_{E}^{cd}$. From the enrichment of the U in the U-Al foils and the percentage of Al present, a per atom activity of the U^{235} can be obtained

$$ \left({}^{i}A_{E}^{cd} / N_{25}^{E} \right) . $$

The U^{235} atom density of the natural uranium foil is also known, N_{25}^{N}, so after volume normalizing, the relative U^{238} fission product activity is given by

$$ {}^{i}A_{28}^{cd} = \left({}^{i}A_{N}^{cd} - \frac{N_{25}^{N}}{N_{25}^{E}} \right) {}^{i}A_{E}^{cd} \quad . $$

This activity, ${}^{i}A_{28}^{cd}$, is corrected by a fraction, $N_{28(fuel)}/N_{28}^{N}$, to obtain the relative activity for a sample having the same U^{238} atom density as the fuel.

To determine the total and relative thermal U^{235} fission product activities, the results from the enriched uranium alloyed with aluminum foils were used. The total activities are represented by ${}^{i}A_{E}^{b}$ and the epithermal by ${}^{i}A_{E}^{cd}$, so the thermal activities are represented by

$$ {}^{i}A_{E}^{th} = {}^{i}A_{E}^{b} - {}^{i}A_{E}^{cd} \quad \text{or} \quad {}^{i}A_{25}^{th} = {}^{i}A_{25}^{b} - {}^{i}A_{25}^{cd} \quad , $$

where the foil activities have been run and mass normalized.

The above results for ${}^{i}A_{28}^{cd}$, ${}^{i}A_{25}^{b}$, and ${}^{i}A_{25}^{th}$ are then corrected to apply to the U^{235} and U^{238} atom density of the U-Mo fuel. The enrichment of the uranium in the U-Al foils is 93.37 w/o, and the foils are 18.7 w/o uranium, the remainder being aluminum. The values used for the atom densities for the various materials are given in Table XI.

TABLE XI

U^{238} AND U^{235} ATOM DENSITIES IN THE VARIOUS MATERIALS

Material	N_{25}	N_{28}
Natural Uranium	0.3427×10^{21}	47.23×10^{21}
Uranium Aluminum	1.438×10^{21}	0.1008×10^{21}
U - 10 w/o Mo Fuel	1.359×10^{21}	37.58×10^{21}
UC Fuel	1.108×10^{21}	30.64×10^{21}

These results are then used to determine $r_{\epsilon 1}$ and $r_{\epsilon 2}$.

The results reported are relative activities. They have all been mass and run normalized and have been corrected for buckling for the lattice in which the measurements were made. The values of the activities measured for the natural uranium foils, cadmium-covered, and the enriched uranium foils both bare and cadmium-covered are listed in Tables XII and XIII. The results are shown for each representative fuel rod for each lattice studied. And the average for the fuel is given in each case.

Using the corrections described above, the values of ${}^{i}A_{28}^{cd}$, ${}^{i}A_{25}^{b}$, and ${}^{i}A_{25}^{th}$ were obtained. Having these results the ratios

$$r_{\epsilon 1} = \frac{{}^{i}A_{28}^{cd}}{{}^{i}A_{25}^{b}} \qquad \text{and} \qquad r_{\epsilon 2} = \frac{{}^{i}A_{28}^{cd}}{{}^{i}A_{25}^{th}}$$

were determined. The results are given in Table XIV.

TABLE XII
MEASURED RELATIVE FISSION PRODUCT ACTIVITIES
IN U - 10 Mo FUEL USED TO DETERMINE r_ϵ

Detector Foil	Lattice	Fission Product Activities $^iA^{cd}$ and $^iA^b$				
		Rod 1	Rod 2	Rod 8	Rod 9	Avg. Fuel ($^i\bar{A}$)
Natural U, Cd-covered	13-in.	13718	14381	15297	15092	14861 ± 102
U-Al	13-in.	66281	74204	100379	104348	91572 ± 206
U-Al, Cd-covered	13-in.	33594	35609	38749	40001	37881 ± 83
Natural U, Cd-covered	16-in.	16952	17309	17561	17472	17421 ± 87
U-Al	16-in.	89067	104997	156218	157322	136857 ± 86
U-Al, Cd-covered	16-in.	35641	36920	41780	42351	40503 ± 67
Natural U, Cd-covered	19-in.	5247	5255	5143	5259	5231 ± 41
U-Al	19-in.	29511	34269	53129	55318	46622 ± 74
U-Al, Cd-covered	19-in.	9673	10522	11330	11478	11035 ± 58

TABLE XIII
MEASURED RELATIVE FISSION PRODUCT ACTIVITIES
USED TO DETERMINE r_ϵ IN THE UC ELEMENT

Detector Foil	Lattice	Fission Product Activities $^iA^{cd}$ and $^iA^b$			
		Rod 1	Rod 2	Rod 3	Avg. Fuel ($^i\bar{A}$)
Natural U, Cd-covered	16-in.	6991	8759	8757	8317 ± 167
U-Al	16-in.	46707	67242	71068	64022 ± 827
U-Al, Cd-covered	16-in.	16818	18437	19236	18432 ± 301
Natural U, Cd-covered	13-in.	3749	3668	3643	3676 ± 84
U-Al	13-in.	16515	21916	23304	21259 ± 271
U-Al, Cd-covered	13-in.	8513	9446	9564	9272 ± 140

TABLE XIV

RELATIVE VALUES OF U^{238} AND U^{235} FISSION PRODUCT ACTIVITIES AND THE RATIOS OF U^{238} FISSIONS TO U^{235} FISSIONS

Lattice	Fuel	$^{i}A_{28}^{cd}$	$^{i}A_{25}^{b}$	$^{i}A_{25}^{th}$	$r_{\epsilon 1}$	$r_{\epsilon 2}$
13-in.	U - 10 Mo	4,508 ± 24	86,540 ± 195	50,740 ± 222	0.0521 ± 0.0014	0.0880 ± 0.0025
16-in.	U - 10 Mo	6,078 ± 117	129,339 ± 104	91,060 ± 103	0.0470 ± 0.0009	0.0667 ± 0.0013
19-in.	U - 10 Mo	2,016 ± 61	44,060 ± 73	33,632 ± 97	0.0463 ± 0.0014	0.0602 ± 0.0018
13-in.	UC	932 ± 83	16,380 ± 288	9,236 ± 180	0.057 ± 0.005	0.101 ± 0.007
16-in.	UC	2,508 ± 214	49,329 ± 743	35,050 ± 724	0.051 ± 0.004	0.072 ± 0.006

X. CONCLUSIONS

The results of these experiments have been used to aid in setting the enrichment of the fuel to be used in the HNPF reactor and to aid in establishing the design of the U - 10 Mo fuel cluster. The values of material buckling were used as a basis for checking the calculational models used for the reactor. One method used to improve the accuracy of the calculation of the required enrichment of fuel for the actual reactor, was to adjust the resonance integral of molybdenum to force agreement of the calculations with the measured values of the material buckling and then use this adjusted value in the calculational model for the Hallam reactor. This method of fitting the value of the resonance integral of molybdenum changed the previously calculated value of k_{eff} by $\sim$ 1-1/2% and was therefore very helpful in the final decision of selecting the fuel enrichment necessary for the Hallam reactor. Experimental values of the resonance integral of molybdenum, reported after this work, agree with the value chosen from the buckling measurements. Therefore, considerable confidence was placed in this procedure. By making this adjustment all the measured values of material buckling were predicted to within 0.8%. Also the comparison of the neutron flux distribution measurements in the 19-rod and 18-rod U - 10 Mo fuel elements aided in the decision to change the design of the Hallam fuel element from 19 rods to 18 rods. This allowed the now empty central stainless steel tube to be used as a support member and provided a structurally improved fuel cluster.

The other lattice parameters, which were measured, are presently being used to compare to theoretically calculated parameters and adjustments are being made to bring the theory and experiment into agreement and therefore improves the calculational methods. The results of the experimental work have been presented in detail in this report so they can be used to aid in future sodium graphite reactor calculations.

REFERENCES

1. F. C. Gronemeyer and T. W. Merryman, "75,000 Kilowatts of Electricity by Nuclear Fission at the Hallam Nuclear Power Facility," AI-5272 (1960)

2. V. A. Swanson, "Construction and Operation of the AE-6 Water Boiler Reactor," NAA-SR-1920 (1957)

3. J. A. Stanley and M. H. Binstock, "Development and Production of Uranium - 10 wt % Molybdenum As-Cast Slugs for HNPF Physics Experiments," NAA-SR-4874 (1960)

4. S. Glasstone and M. C. Edlund, "The Elements of Nuclear Reactor Theory," D. Van Nostrand Co., Inc., New York (1952) p 123

5. H. Kouts, "Resonance Escape Probability Measurements," BNL-2077 (Declassified) October 30, 1953

6. D. Klein et al., Nuclear Science and Engineering 3, (1958) p 403

7. C. H. Skeen, "Resonance Escape Probability of a Lattice of Multi-Rod Fuel Elements," NAA-SR-3211 (August 1, 1959)

8. C. H. Skeen, Private Communication